

FEATURE ARTICLE

Metal Films with Arrays of Tiny Holes: Spectroscopy with Infrared Plasmonic Scaffolding

James V. Coe,* Kenneth R. Rodriguez, Shannon Teeters-Kennedy, Katherine Cilwa, Joseph Heer, Hong Tian, and Shaun M. Williams

The Ohio State University Department of Chemistry, 100 West 18th Avenue, Columbus, Ohio 43210-1173

Received: April 13, 2007; In Final Form: June 15, 2007

The extraordinary infrared transmission effect of metal films with arrays of tiny holes (microarrays or mesh) is mediated by surface plasmons. This work describes the optical physics of propagating infrared surface plasmons on mesh and reviews initial applications of the effect. In particular, surface-plasmon-enhanced infrared absorption spectroscopy is featured. Contents include: a brief history of surface plasmons, mesh-based surface plasmons, propagating surface plasmon basics, surface plasmon resonance response to nanocoatings, enhanced IR absorption spectroscopy, and the interaction of surface plasmon resonances with molecular vibrations.

1. Introduction

Conducting electrons of a metal act like a plasma and can support surface waves, the quantum of which is known as a surface plasmon (SP). SPs have been described as light trapped at the metal surface and, in that sense, can be considered as two-dimensional light. The prospect of manipulating SPs in nanostructures of low dimensionality and subwavelength spaces¹ offers many interesting properties and applications including (to name only a few) generation of shorter wavelengths than the incident radiation leading to sub-diffraction-limit imaging,² superlensing,^{3,4} importance in near field scanning optical microscopy (NSOM),⁵ high surface electric fields,^{6,7} for surface enhanced Raman spectroscopy^{8–10} (SERS), potential for bridging photonics and electronics,^{11,12} SP resonance sensors (SPR) for bioanalytical assays,¹³ more efficient collection of fluorescence^{14,15} using SP coupled emission (SPCE), and extraordinary optical transmission of nanoarrays.¹⁶ The last of these has led to enhanced direct infrared (IR) absorption spectroscopy¹⁷ of nanoscale coatings on microarrays, the subject of this article.

1.1. Brief History of Propagating SPs. A historical perspective on SPs can be gained from Maystre's collection of selected papers.¹⁸ Though not yet denoted as SPs, anomalies in the performance of Rowland's high resolution, speculum diffraction gratings were first described in 1902 by Wood¹⁹ and later (1936) by Strong.²⁰ Rapidly changing features in Wood's spectral anomalies were recognized by Lord Rayleigh²¹ as interference effects, now called Rayleigh edges. In 1941 Fano²² presented a theoretical description of SPs as "polarized quasi-stationary waves which represent an energy current rolling along the surface of a metal". Interestingly, Fano also related the problem to an antenna near a metal surface (now the hot topic of SPCE) as originally addressed theoretically by Sommerfeld.²³ SPs were predicted^{24,25} and observed^{26–28} with electron loss spectra in the late 1950s and early '60s. Teng and Stern²⁹ described the bombardment of gratings (rather than smooth metal surfaces)

with 10 keV electrons producing photons and characteristic SP dispersion curves. Note that light cannot match the momentum of SPs at any incident angle on a smooth air/metal interface,³⁰ and as a result, prisms, gratings, dipoles, or surface roughness are needed to excite SPs with light. Ritchie et al.³¹ showed how to make SP dispersion measurements by varying the angle of incident light on diffraction gratings and described the Lorentzian nature of the SP as an intermediate state in a photon absorption/re-emission process. Around 1973, Hutley and Bird³² connected the light seen by Teng and Stern using electron beam excitation to the light-based grating work establishing the cause of Wood's anomalies as SPs. While SPs are not yet textbook material, they will rapidly become so. The field of propagating SPs took off in the late 1960s when Otto,³³ followed closely by Kretschmann and Raether,³⁴ demonstrated SP attenuated total reflection (SP ATR, sometimes called SPR).³⁰ These experiments reflect a fixed-frequency laser from a metal-coated prism with monitoring of a dip in reflected intensity (when SPs are excited) as a function of incident angle. A recent SciFinder search on "surface plasmon reviews" found 479 hits, so SP material abounds, and we mention only a few SP reviews^{35,36} and a few SP ATR accounts^{30,37,38} that will be related to hole arrays.

1.2. Metal Films with Arrays of Tiny Holes. Metal films with arrays of holes are now considered new plasmonic metamaterials;³⁹ however, the history goes back to 1974 when Ulrich⁴⁰ demonstrated and theoretically described a transmission resonance in the far-infrared region ($\sim 80\text{ cm}^{-1}$) of electroformed, freestanding Cu mesh with a square lattice of square holes (hole-to-hole spacing of $101\ \mu\text{m}$, hole width of $87\ \mu\text{m}$, and thickness of $5\ \mu\text{m}$, see Figure 2 therein). He called the transmission resonances "leaky guided modes", described a splitting due to coupling of the surface waves on the front and back sides of the mesh, attributed the resonance widths to loss by radiation damping, and observed dispersion of a single, asymmetric, broad transmission resonance at perpendicular incidence into three peaks at an incident angle of 30° . Regarding

* To whom correspondence should be addressed. E-mail: coe.1@osu.edu.



From left to right: Kenneth R. Rodriguez, Shannon Teeters-Kennedy, James Coe, Katherine Cilwa, Hong Tian, and Joseph Heer.

Jim Coe received his B.A. with Honors in 1980 from Swarthmore College and his Ph.D. in 1986 from The Johns Hopkins University (advisor Kit H. Bowen). Postdoctoral work was done at the University of California, Berkeley (advisor Richard J. Saykally). He is a Professor of Chemistry at The Ohio State University and has been there since 1989. Interests include the optical physics and applications of subwavelength hole arrays in chemistry and spectroscopy, as well as the connection of the properties of finite size materials, like clusters, to bulk.

Kenneth R. Rodriguez received his B.S. in Chemistry from California State University Dominguez Hills in 2001 and M.S. in Chemistry from The Ohio State University in 2005. He is currently finishing his Ph.D. in Physical Chemistry at The Ohio State University under Dr. James V. Coe. His graduate research focuses on IR extraordinary transmission of metallic microarrays to investigate monolayers, bilayer lipid membranes, catalytic reactions, thin films of TiO₂ and carbon, and the interactions of a molecular vibration with a surface plasmon resonance.

Shannon Teeters-Kennedy received B.A. degrees from Capital University in Chemistry and Comprehensive Science Education in 1998. She completed a M.S. in Chemical Physics in 2004, and a Ph.D. in Chemical Physics in 2007, both under the direction of Dr. James V. Coe at The Ohio State University. She has accepted an Assistant Professor position at Franklin College starting in the 2007–2008 school year. Her research interests focus on applications of surface plasmons in stacked mesh and in model membrane systems.

Katherine Cilwa received her B.S. degree in Chemistry, Marine Science minor, from Coastal Carolina University in 2003. She is currently a Ph.D. candidate at The Ohio State University in James Coe's group with a research focus on IR surface plasmon applications.

Joseph Heer graduated with B.S. and M.S. degrees in Chemical Engineering from Case Western Reserve University in 1989 and 1999, respectively. He is currently a Ph.D. student in the Coe group. His research interests include theory and applications of surface plasmons and IR microspectroscopy of single hole systems.

Hong Tian was born in Xinxiang, China, in 1978. She received a B.S. in Chemistry from Zhengzhou University in 1998 and a M.S. in Physical Chemistry in 2001 from Lanzhou Institute of Chemical Physics, Chinese Academy of Sciences. She is currently pursuing her Ph.D. in Analytical Chemistry at The Ohio State University under the guidance of Dr. Richard L. McCreery and Dr. James V. Coe. Her main research interests are surface spectroscopy, electrochemistry, and application of molecular electronics.



Shaun M. Williams received his B.A. in Chemistry from Capital University in 2000. He completed his Ph.D. in Chemical Physics at The Ohio State University in 2006 under Dr. James V. Coe. He is currently an Assistant Professor at Lenoir-Rhyne College in Hickory, NC. His research focuses on the theory of surface plasmons in mesh systems.

utility for SERS, Glass et al.⁶ performed calculations in 1983 on sinusoidal biperiodic metal gratings regarding SP reflectivity resonances (800 nm lattice, 514.5 nm wavelength of light, and Ag dielectric constants). They calculated surface electric field enhancements on resonance of almost 300 over the incident beam. This area of research took off in 1998 when Ebbesen and co-workers¹⁶ fabricated square arrays of cylindrical holes in metallic films (900 nm hole-to-hole spacing, 150 nm hole diameters, 200 nm thickness of silver) and measured unexpectedly large resonant transmissions in the visible and near IR regions. The metal in these films was optically thick, so transmission occurred only by virtue of the perforations. The transmission maximum (@ 1370 nm) occurred at nearly ten times the diameter of an individual hole, twice the fraction of open

hole surface area, and ~1000 times greater than the Bethe limit⁴¹ (an expectation for non-SP-mediated transmission with isolated subwavelength holes and infinitely thin perfect conductors). The effect involves the excitation of SPs by subwavelength structures in the periodic lattice, propagation of SPs along the metal surface and reflection at holes (i.e., a band structure),^{16,42–44} propagation on both sides of the periodic lattice by tunneling through the holes (producing a splitting),^{40,45–47} and finally a conversion of SPs back into photons by radiation damping at the hole structures,^{48–50} probably involving the localized SP properties of the holes.^{51,52} The Ebbesen *Nature* paper led to a profusion of work (it has been cited 1003 times at the time of writing) and this phenomenon has been dubbed “Ebbesen’s extraordinary transmission effect” or “extraordinary optical transmission” (EOT). The shape of the holes^{51,53,54} and relation to the lattice^{55,56} are very important. Square holes are considerably better than circular holes⁵³ when normalized for open area suggesting that shape resonances (i.e., localized SPs) are at play in EOT. Hexagonal arrays seem to have larger EOT than square lattices⁴⁸ when normalized for area of commonly shaped holes. Metal mesh arrays have been investigated by ultrafast pulses,⁵⁷ entangled photon pairs⁵⁸ showing the true quantum mechanical nature of mesh SPs, polarization studies^{59,60} revealing non-locality and conditions preserving or degrading polarization involving propagating SPs, and near field imaging.⁴⁴

After many years of intense research, no grand consensus about the EOT effect has emerged from theory. Popov et al.⁶¹ have pointed out that there is an efficient channel in lamellar

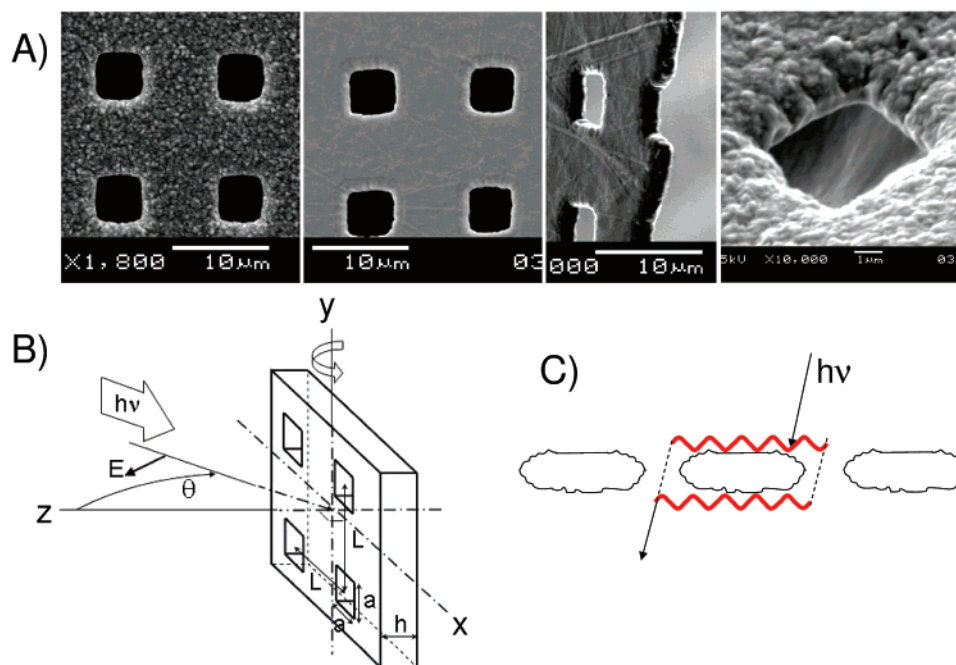


Figure 1. (A) Scanning electron microscope images of the back, front, side, and individual microchannel of a typical Ni mesh. The white bars are $10\ \mu\text{m}$ in the first three images and $1\ \mu\text{m}$ in the last. The lattice parameter (L) is $12.7\ \mu\text{m}$, the hole width (a) is $\sim 5\ \mu\text{m}$, and the width (h) is $\sim 3\ \mu\text{m}$. (B) Definition of mesh geometrical parameters and the orientation of incident light in the ΓX configuration. (C) Cartoon of incoming and outgoing radiation with SPs represented as red wiggly lines.

gratings that does not exist for two-dimensional (2D) hole arrays, so the many calculations on 1D arrays of slits may not be helpful for grid structures. Martin-Moreno et al. gave an early theory of the lineshape of an infinite grid at perpendicular incidence⁶² based on tunneling between SPs on each side. They found two resonance features (for thicknesses less than the hole width) including a sharp resonance at a wavelength near the hole-to-hole spacing. Other recent theoretical grid studies^{63,64} find a propagating SP mode that is hybridized with the local modes of the hole enabling Fabry–Perot behavior (as previously discussed by Martin-Moreno et al.⁶² and foreshadowing effects described in section 3.4). Bravo-Abad et al. performed calculations on 1D chains of subwavelength holes in perfect conductors and found EOT. They found both a broad and a sharp resonance for infinite chains, whereby the sharp one (at a wavelength near the hole-to-hole spacing) lost intensity in finite chains. They suggest that chains of holes are the basic geometrical unit of EOT. Since SPs require an imaginary component to the metal's dielectric,³⁰ these studies purport “surface EM modes” rather than SPs. Such states may disperse differently^{39,65} than propagating SPs, so experimental polarized characterization of the mode dispersion is vital regarding the role of SPs.^{43,66}

Certain experiments are particularly telling with regard to the role of SPs, such as polarized dispersion studies in reflection, absorption, and transmission⁴³ and the double stack experiments herein of section 2.4. Near-field imaging experiments by Devaux et al.⁶⁷ have launched SPs (with light perpendicularly incident on a grid nanoarray) across $30\ \mu\text{m}$ of flat metal surface, to a second grid nanoarray where light couples back out, again perpendicular to the surface. These experiments demonstrate the feasibility of SP photonic circuits as well as demonstrating a role for SPs in the EOT mechanism. Murray et al.⁶⁸ have fabricated metal nanoparticles of increasing width on a fixed grid such that, at some point, the nanoparticles merge into a continuous metal film perforated by holes. They observe a transition from localized SPs to propagating SPs as indicated by substantial shifts in the frequency of the transmission

resonances. Patterned arrays of metal films offer a rich array of SP phenomena that may be fruitfully integrated into sensors and spectrometers.

1.3. Metal Films with Arrays of Tiny Holes in the IR. After the pioneering FIR work of Ulrich,⁴⁰ there have been experimental and computational studies by Moller et al.^{69,70} of grids with cross-shaped holes showing transmission resonances in the IR attributed to “excited surface waves coupled by waveguide modes of the openings”. Ebbesen's extraordinary transmission effect was moved into the IR by the Coe group in order to overlap with the fundamental vibrations of molecules.⁷¹ Scanning electron microscope (SEM) images of typical freestanding metal films (meshes) that support propagating SPs in the IR are shown in Figure 1A. Geometrical parameters are defined in Figure 1B and a cartoon of the transmission process is given in Figure 1C with the propagating SPs indicated with red wiggly lines. Dispersion curves, resonance lineshapes, splittings, and other basic optical physics of SP transmission resonances were also studied.^{45,66,71–74} SP-enhanced IR absorption spectroscopy (herein called SPEIRA on mesh, see section 3.1) facilitates the recording of spectra of self-assembled monolayers,^{17,72,74} phospholipid bilayers,^{66,72,74,75} and catalytic surface reactions.^{72,76–78} Lee and co-workers have fabricated metal microarray grids on silicon observing dispersion and splittings of SPs,^{46,47} a grid based thermal emission device⁷⁹ with remotely coupled SPs,^{80,81} and a crucial role of SPs for contrast improvement in Moire fringes.⁸²

2. SP Basics

Dispersion curves are key to understanding SP-mediated transmission resonances on metal mesh. They are plots of SP angular frequency ($\omega = 2\pi/\lambda$) vs momentum wavevector parallel to the surface (k_x in Figure 2 for geometry of Figure 1B). We typically use the proportional quantity, the reciprocal wavelength (or wavenumber), $\tilde{\nu} = \omega/(2\pi)$, due to our interest in IR spectroscopy. The dispersion curve of a propagating SP on a

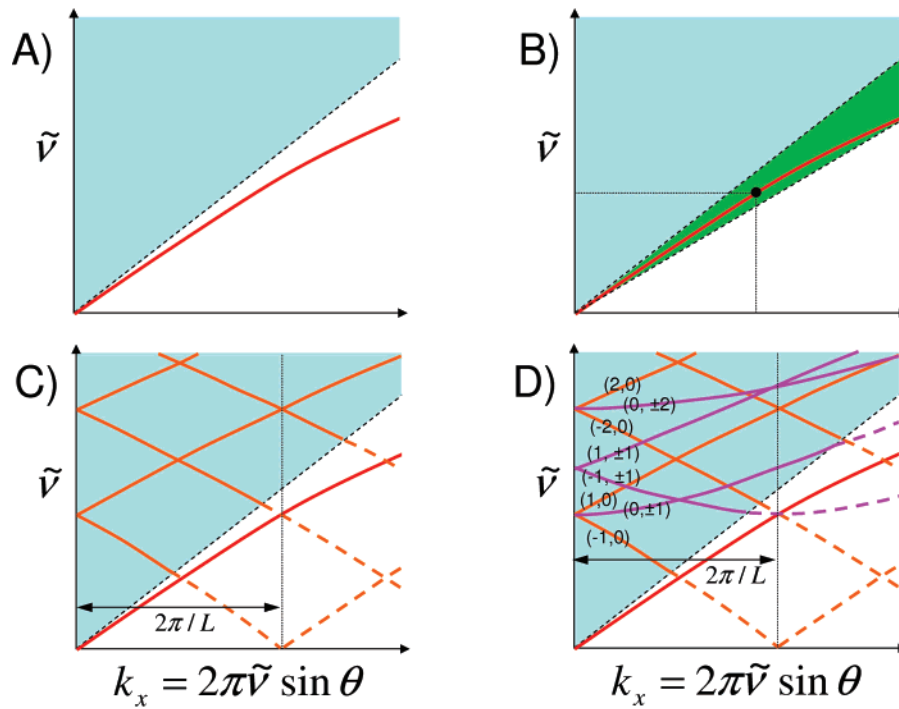


Figure 2. Dispersion diagrams showing the SP dispersion curve (red), the light line (dotted), and the region that is accessible by varying the angle of incident radiation (light blue). (A) Smooth air/metal interface where the SP curve lies outside of the light line and is not accessible. (B) A smooth nanocoating of metal on a prism (SP ATR configuration). The green region is additionally accessible by the index of refraction of the prism and overlaps with the SP dispersion curve which is now accessible by light. (C) 1D array of slits or grating. Periodicity projects (in units of $2\pi/L$) the SP dispersion curve inside the light line yielding the orange curves. (D) 2D array of holes or bigrating. There can also be momentum in the y -direction which additionally gives rise to the purple curves when projected into the k_x coordinate.

smooth air/metal interface is given in red in Figure 2A. Incident radiation (at an angle of θ from the z axis along the x axis, see Figure 1B) can only access the blue region in Figure 2A since the momentum wavevector component of light parallel to the surface is $k_x = 2\pi\tilde{\nu} \sin \theta$. The dotted line in Figure 2A is called the “light line”, its formula is $\tilde{\nu} = k_x/(2\pi)$, and it corresponds to the momentum wavevectors obtainable if light were brought in parallel to the surface. Optical physicists say the SP dispersion curve (red line) lies outside the light line which means that there is no angle of incident radiation that can excite SPs on a smooth air/metal interface. In other words, SPs have momentum greater than incident photons at the air/metal interface, so some feature of the interface must add momentum to the photons in order to match that of SPs. Typically prisms, gratings, or surface roughness are used to couple light to SPs.³⁰ The placement of a smooth metal film on a prism (by virtue of the prism’s increased index of refraction relative to air) increases the region accessible by angle tuning of incident radiation as shown in green in Figure 2B. There are specific angles which will couple the light of fixed wavelengths and SPs (see the vertical and horizontal dotted lines in Figure 2B) giving rise to a reflectivity resonance as a function of angle (the basis of SP ATR experiments discussed near the end of section 1.1). If, instead of using a prism, the metal film is corrugated with a periodic pattern of slits, then the surface can transfer momentum in units of $2\pi/L$. The SP dispersion curve manifests itself with a Brillouin periodicity resulting in access within the light line as shown with orange curves in Figure 2C. Since the meshes of this work are bi-gratings having holes in both the x and y directions, they gain momentum in units of $2\pi/L$ in either the x or y directions, i.e., as the magnitude of $(2\pi/L)i\hat{x} + (2\pi/L)j\hat{y}$ where i and j both label the resonances (i,j) and are steps along the reciprocal lattice. A coordinate system and geometrical parameters are defined for a mesh with a square lattice of square holes in Figure

1B, where L is the lattice parameter (hole center-to-hole center spacing), a is the square hole width, h is the thickness of the film, with holes aligned along the x and y axes, and light incident along the z axis when $\theta = 0^\circ$. Momentum gained from the y component projects into the k_x picture of Figure 2 giving rise additionally to the purple curves in Figure 2D. The transmission resonances at low momentum wavevectors are labeled by (i,j) as seen in Figure 2D. Bigratings have a number of features different than their 1D analogs, including a higher density of resonances, some resonances (purple ones) with different dispersion, and some with different polarization properties. Useful transmission is observed over the whole range of fundamental molecular vibrations for the meshes with geometry of Figure 1A.

2.1. Front-Back Coupling and SP Dispersion Curves of Mesh. A SP dispersion curve (red curve in Figure 2) is given in momentum space as

$$\tilde{\nu}_{\text{SP}}(k_x) = \frac{k_x}{2\pi n'_{\text{eff}}(\tilde{\nu})} \quad (1)$$

where n'_{eff} is the real part of the effective index of refraction of the interface (a function of wavelength). In order to gain intuition, assume that n'_{eff} is a simple function of wavelength, such as $n'_{\text{eff}} = m\tilde{\nu} + b$. The analytical expression for eq 1, under this assumption, is

$$\tilde{\nu}_{\text{SP}}(k_x) = \frac{-b + \sqrt{b^2 + 4m\left(\frac{k_x}{2\pi}\right)}}{2m} = \frac{1}{2\pi b}k_x - \frac{m}{4\pi^2 b^3}k_x^2 + O(k_x^3) \quad (2)$$

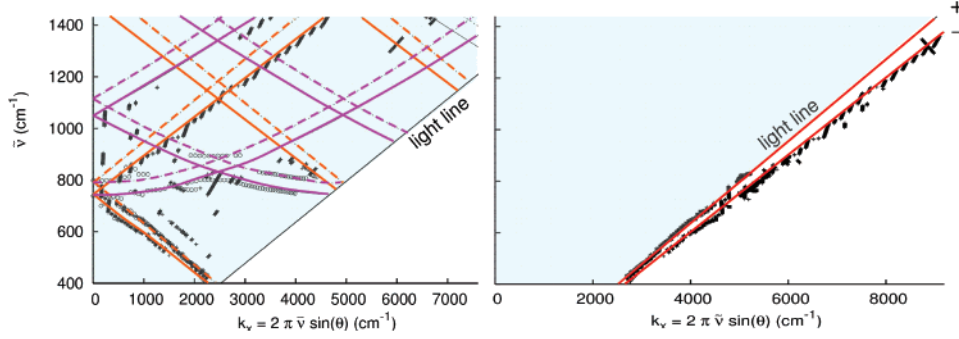


Figure 3. Measured positions of transmission resonances (left) of mesh shown in Figure 1A and modeled dispersion curves with the same color coding as in Figure 2D. With assigned values of i and j , the peaks were projected just outside of the light line. They fell onto two SP dispersion curves (shown with red) illustrating the effect of front-back coupling of SPs through the holes.

In the IR with our type of meshes, m and b are positive and $m \ll b$, so this function has a “light line”-like linear term with a downward quadratic distortion (as drawn in red in Figure 2). A derivation based on bigrating momentum matching⁶⁵ gives the corresponding transmission resonances (orange and purple lines in Figure 2D), under the $n'_{\text{eff}} = m\tilde{\nu} + b$ assumption, as

$$\tilde{\nu}_{(i,j)}(k_x) = \frac{-b + \sqrt{b^2 + 4m\sqrt{\left(\frac{k_x}{2\pi} + \frac{i}{L}\right)^2 + \left(\frac{j}{L}\right)^2}}}{2m} \quad (3)$$

At perpendicular incidence ($k_x = 0$) and going back to the more general relation [in the limit as $m \rightarrow 0$, $b(\tilde{\nu}) \rightarrow n'_{\text{eff}}$], the resonances occur at^{45,66}

$$\tilde{\nu}_{(i,j)\pm}(k_x = 0) = \frac{\sqrt{i^2 + j^2}}{Ln'_{\text{eff},\pm}} \quad (4)$$

Mesh with a thickness less than the wavelength of incident radiation may exhibit a splitting of each resonance (indicated by the “+” or “−” subscript of the labels) due to the coupling of the propagating SPs between the front and back surfaces of the mesh through the holes. As shown in Figure 3, we discovered this by painstakingly assigning (i,j) values to observed transmission resonances (left side of Figure 3) and projecting⁴⁵ them onto corresponding SP dispersion curves (right side of Figure 3). Note that Figure 3 has the same color coding as Figure 2D. The peaks project onto two SP dispersion curves (red), one close to the light line (the “+” curve) and one displaced to higher momentum (the “−” curve) by the strong radiation damping of the mesh. The parameter $n'_{\text{eff},+}$ [from eq 4] is 1.000 for most all air/metal interfaces in the IR [based on $n'_{\text{eff}} = \text{Re}\{[\epsilon_m \epsilon_s / (\epsilon_m + \epsilon_s)]^{1/2}\}$ where ϵ_m and ϵ_s are the complex dielectrics of the metal and substrate, respectively^{30,37}]. The value of $n'_{\text{eff},-}$ is about 1.06 for the data in Figure 3. Confidence can be gained in eq 4 by examining the labeled resonances in zero-order, transmission spectra at perpendicular incidence as shown in Figure 4 (for the same mesh imaged in Figure 1A). The position of the $(1,0)_+$ resonance at $\tilde{\nu}_{(1,0)_+} = 789.2 \text{ cm}^{-1}$ and $n'_{\text{eff},+} = 1.000$ determines a value of $L = 12.7 \mu\text{m}$ which is in agreement with independent SEM measurements. Furthermore, the ratio $\tilde{\nu}_{(1,1)_+}/\tilde{\nu}_{(1,0)_+} = 1116.0/789.2 = 1.4140$ is within 0.01% of the $\sqrt{2}$ as predicted by eq 4. Both resonances are observed with our mesh, but the “−” resonances are much more intense than the “+” resonances. The split SP dispersion curves of the sort shown in Figure 3 are well-known in SP ATR experiments involving the coupling between adjacent, smooth air/metal interfaces with wavelength-scale spacings.^{30,38,66,83–85} The “−” resonances have opposite charge distributions on

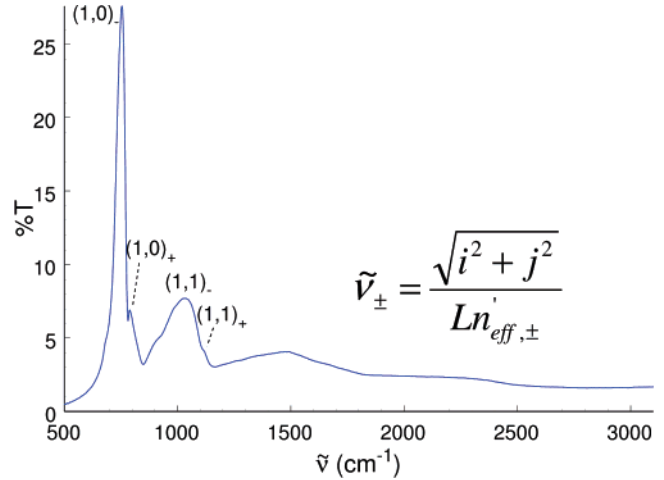


Figure 4. Zero-order transmission spectra at perpendicular incidence of the Ni mesh pictured in Figure 1A. Front-back coupling through the holes of the mesh is evident in the splitting of the two largest resonances (“+” and “−” pairs). The $(1,0)_-$, $(1,0)_+$, $(1,1)_-$, and $(1,1)_+$ resonances occur at 754.7, 789.2, 1034.8, and 1116.0 cm^{-1} , respectively.

opposing interfaces giving rise to stronger electric fields in the material separating the interfaces. When such materials are absorbing, like metal, they tend to attenuate “−” modes,^{38,84} whereas nonabsorbing materials, like air, tend to favor them. Seeing a large “−” mode with mesh suggests (as is already known) that the SPs couple through the air-filled holes. Such splittings on mesh have also been observed by Lee and co-workers^{46,47} for thin metal grids deposited on silicon.

If the splitting due to front-back coupling through the holes can be observed at perpendicular incidence, then there is a simple way to determine SP dispersion curves.⁶⁶ The right side of Figure 3 reveals that a positive shift from the “+” SP dispersion curve to the “−” SP curve along the momentum coordinate (k_x) corresponds to negative shift (or red shift) from the “+” resonance to the “−” resonance in frequency space at perpendicular incidence on mesh. The positions of the more intense $(1,0)_-$ and $(1,1)_-$ resonances are shifted to considerably lower frequencies from their “+” partners due to strong front-back coupling through holes on the mesh. The observed positions [see caption of Figure 4 and eq 4] correspond to $n'_{\text{eff},-} = 1.0458 @ 754.7 \text{ cm}^{-1}$ and $n'_{\text{eff},-} = 1.0787 @ 1034.8 \text{ cm}^{-1}$, which solved for k_x with eq 2 gives $k_x = 4958 \text{ cm}^{-1} @ \tilde{\nu} = 754.7 \text{ cm}^{-1}$ and $k_x = 7014 \text{ cm}^{-1} @ \tilde{\nu} = 1034.8 \text{ cm}^{-1}$. This corresponds to eq 2 parameters of $b = 1.027$ and $m = 9.733 \times 10^{-5} \text{ cm}$ for the “−” SP curve. The “+” SP curve is just $k_x/(2\pi)$. Note that the SP dispersion curve in momentum space has been determined without varying the angle of the mesh, just by observing the splitting of two resonances.

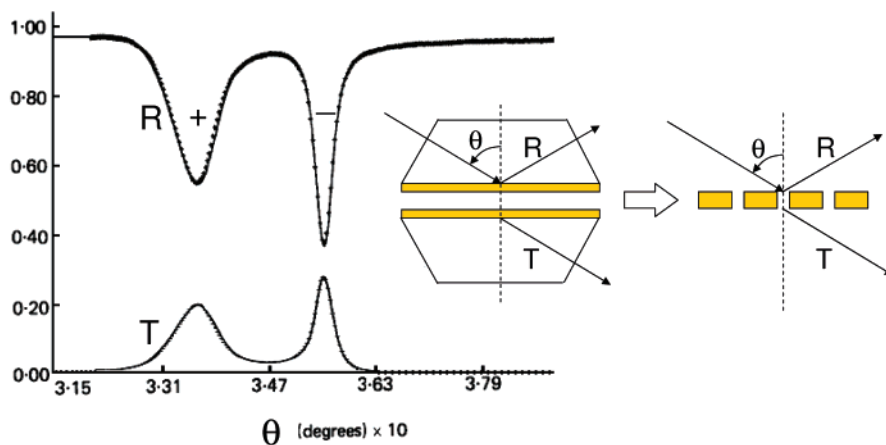


Figure 5. Reflectance and transmittance vs incident angle (θ) of a stack of two SP ATR prisms from the work of Welford and Sambles. The observation of two resonance features (and transmission itself) is due to coupling between the two air/metal interfaces. Analogous behavior (as shown at right) is seen with a simple piece of mesh due to front-back coupling through the holes.

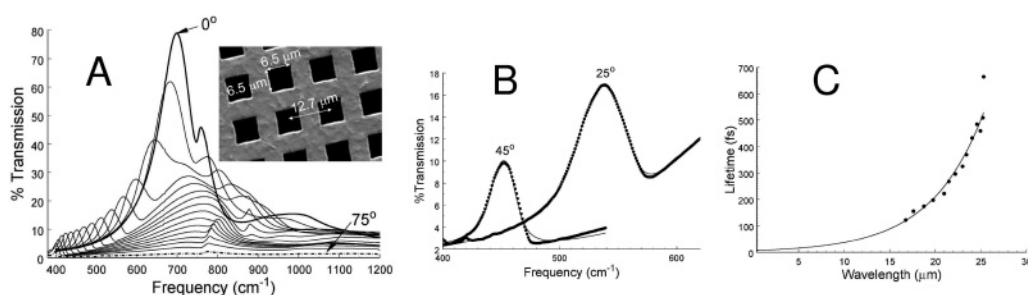


Figure 6. (A) Transmission spectra upon angling Ni mesh from 0 to 75° in 5° steps relative to the incident beam (IX geometry) showing dispersion. This mesh had larger holes (6.5 μm) than that of Figure 1A, but a similar lattice. (B) The $(-1,0)$ -resonance was isolated by angling and fit to a damped harmonic oscillator model. (C) The damping lifetimes were found to depend exponentially on wavelength with a constant determined by the width of the holes.

But, why is this important? Many theoretical and experimental results concerning propagating SPs are associated with SP ATR experiments.^{30,33,34} The dips in reflected intensity are very much related to the upswings in transmitted intensity seen with our mesh arrays. This can be illustrated by considering the optical work of Welford and Sambles³⁸ on a stack of two SP ATR prisms (configured with a wavelength scale spacing as shown in the inset of Figure 5). Although a single SP ATR prism shows only one reflectivity resonance, the addition of a second coupled SP ATR prism gives a pair of resonances, both observable in reflection and transmission. A single piece of metal film with an array of holes is in many ways the functional equivalent of a stack of two coupled SP ATR prisms, i.e., both coupling of the front and back interfaces on mesh arrays as well as prominent transmission is observed, just like with the stacked prisms. Of course, a mounted assembly of two carefully coated prisms might cost thousands of dollars, whereas a 3 mm \times 3 mm piece of our mesh costs \sim \$.3 (from Precision Eforming). With a SP dispersion curve, the theoretical predictions or experimental results from SP ATR work in momentum space, such as Pockrand's second-order theory³⁷ on nanocoatings (section 2.3), can be converted to expectations in frequency space at perpendicular incidence for mesh (or vice versa).

Although there is utility and simplicity in determination of the SP dispersion curves without angling, there are also situations when angling of the mesh is useful in tuning the positions of transmission resonances (see section 3.4). The orientation described in Figure 1B (and Figures 2D and 3) is denoted IX. Rotation of the mesh in Figure 1B by 45° about the z axis gives the ΓM configuration. The difference of dispersion in the IX and ΓM orientations has been presented

previously.⁷³ Williams⁶⁵ (appendix B therein) has given a general equation based on SP momentum matching for the frequency of (i,j) transmission resonances at any arbitrary angles of the mesh relative to the incident beam.

2.2. IR SP Properties of Mesh. The intrinsic resonance line width³⁰ of propagating SPs on a smooth air metal interface is proportional to $\epsilon''_m/\epsilon'_m{}^2$ where the complex dielectric of the metal is $\epsilon_m = \epsilon'_m + i\epsilon''_m$, so it is important to have $|\epsilon'_m| > \epsilon_m$ for narrow resonances. Rakic et al.⁸⁶ have provided Lorentz-Drude modeling of the complex dielectric constant data for 11 different metals enabling values to be determined at any wavelength from the ultraviolet to the IR. Note that Williams has also given polynomial fits of this work that are valid in the IR region and do not require software that handles complex algebra.⁶⁵ The dielectric properties of metals can be very different in the IR⁷¹ than in the visible where the vast amount of SP work is performed. For instance, the dielectric constant of gold is $-12.4 + i2.4$ (@ 632 nm, 1.96 eV, or 15 800 cm^{-1}) but $-4881 + i2621$ (@ 12 500 nm, 0.099 eV, or 800 cm^{-1}). Although Ag, Au, and Cu are the most common metals for SP work in the visible, many different metals will work in the IR including Ni, Cr, W, Pt, and Pd. This bodes well for the study of catalytic reactions at metal surfaces (see section 3.2). The mesh as in Figure 1B is only commercially available (from Precision Eforming) in Ni which becomes SP active below \sim 4400 cm^{-1} leaving the mid-IR region available for SP enhanced vibrational spectroscopy of molecules at the Ni interface.⁷¹

The dispersion of transmission resonances in the IX configuration⁷¹ is shown in Figure 6A for Ni mesh like Figure 1B, but with larger hole widths ($a = 6.5 \mu\text{m}$). These scans

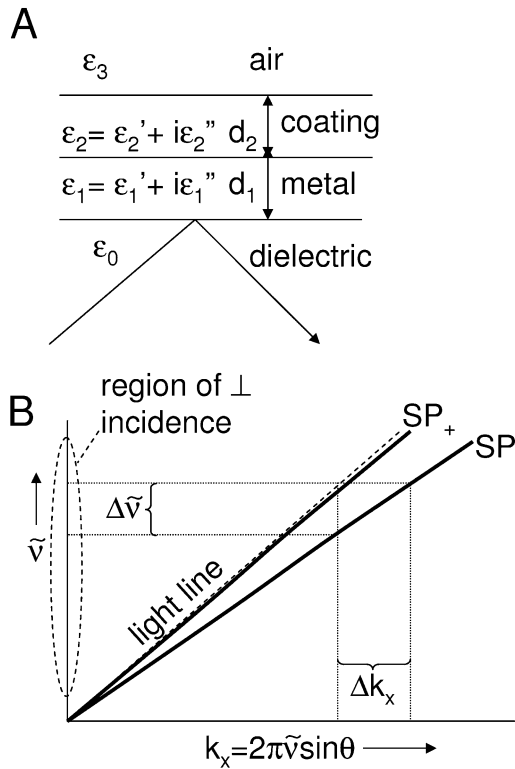


Figure 7. (A) Dielectric properties and geometry of typical SP ATR setup used in Pockrand's theory for reflection resonances. (B) A dispersion diagram with two split SP dispersion curves showing how theory (as that of part A) describes positive shifts in momentum space (Δk_x) which correspond to negative shifts ($\Delta\tilde{\nu}$) at perpendicular incidence, such as when doing spectroscopy on mesh.

correspond to a range from $\theta = 0$ to 75° in 5° increments. The primary resonance is ~ 100 times broader than the intrinsic limit, which we now know to be due to radiation damping, basically SPs get to the next hole (or so) and come back out as radiation. The $(-1,0)_-$ resonance can be isolated from the others at lower frequencies using angles greater than 15° . In this region, the front-back coupling is considerably smaller and it was possible to fit this isolated resonance to a single damped harmonic oscillator model (see Figure 6B) giving the damping lifetimes shown in Figure 6C. At $\sim 15^\circ$ incidence, the 120 fs lifetime of the $(1,0)_-$ SP-mediated resonance corresponds to propagation of $34 \mu\text{m}$ (at 94% of the speed of light in vacuum) which can be a useful effective path length for absorption spectroscopy. The effect of hole width and depth has been studied in the visible region⁸⁷ and in the IR.⁷³ There is an exponential dependence with wavelength (see Figure 6C), and we now realize that the reciprocal of the $1/e$ constant previously found⁷¹ is about the hole width (a). For a fixed lattice parameter, the resonances get narrower and the front-back coupling gets smaller as the holes get smaller.⁷³ When the holes are smaller than $\sim (1/4)L$, the transmission resonances stop dispersing like propagating SPs and exhibit flat dispersion which we now attribute to localized SPs that are associated with the shape of the hole (we mislabeled this effect in ref 73).

2.3. Nanoscale Coatings. IR plasmonic meshes respond to the application of molecules both in terms of changes to the position and width of transmission resonances, as well as enhancements in molecular absorptions (subject of section 3.1). Pockrand's SP ATR work on metal films with absorbing and nonabsorbing coatings³⁷ provides important guidance in interpreting the mesh results (see the geometry and notations for SP ATR defined in Figure 7A where a subscripted "1" refers

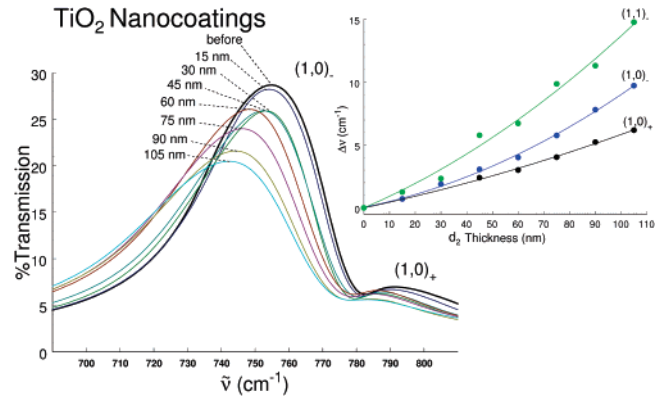


Figure 8. Zero-order transmission spectra at perpendicular incidence (bottom left) of TiO₂ nanocoatings of different thicknesses on Ni mesh. The negative of the shift of several resonances [$(1,0)_-$, $(1,0)_+$, $(1,1)_-$] from their positions on uncoated mesh is plotted against thickness on the upper right. The “-” resonances are more sensitive to nanocoatings, but there is a need for theoretical characterization of the effect.

to the metal film, “2” to the coating, and “0” and “3” to the surrounding dielectrics). The idea here is to take a shift in momentum wavevector predicted by SP ATR theory and use it (with knowledge of the SP dispersion curve) to predict a shift in frequency space at perpendicular incidence as shown in Figure 7B. Pockrand's general second order equation for momentum wavevector is³⁷

$$\underline{k}_x = \underline{k}_x^{(0)} + \underline{k}_x^{(1)C} + \underline{k}_x^{(2)C} + \underline{k}_x^{(1)R} + \underline{k}_x^{(2)R} + \underline{k}_x^{(2)CR} + \dots \quad (5)$$

where $\underline{k}_x^{(0)}$ gives the well-known, zero-order dispersion of SPs at a smooth metal/dielectric interface $Re\{k_x^{(0)}\} = Re\{2\pi\tilde{\nu}(\epsilon_1\epsilon_2)/(\epsilon_1 + \epsilon_2)^{1/2}\}$, $\underline{k}_x^{(1)C} + \underline{k}_x^{(2)C}$ are the first and second order terms due to the coating, $\underline{k}_x^{(1)R} + \underline{k}_x^{(2)R}$ are the first- and second-order terms due to radiation damping, $\underline{k}_x^{(2)CR}$ is a second-order term describing the interaction of the coating and radiation damping, and underlined quantities are complex. Explicit expressions are given by Pockrand for each of these terms. The first three terms on the right-hand-side of eq 5 may be directly applicable to the mesh results; however, the latter three terms on the right-hand-side are not [as the radiation damping of mesh (front-back coupling through the holes) is different than the radiation damping of SP ATR experiments (thinness of a smooth metal film enabling coupling between the two smooth dielectric/metal interfaces)]. Although the $(i,j)_+$ resonances of our mesh are considerably less intense than the $(i,j)_-$ resonances, they are easier to model because they are not affected by radiation damping and the interaction of coatings with radiation damping. The frequency shifts of the “+” resonances at perpendicular incidence are obtained using Pockrand's absorbing coating expressions³⁷ for $\underline{k}_x^{(1)C} + \underline{k}_x^{(2)C}$ with collection of terms on the coating thickness (\overline{d}_2) (for a SP curve close to the light line) as

$$\Delta\tilde{\nu}_+ = C\tilde{\nu}^2 d_2 + D\tilde{\nu}^3 d_2^2 \quad (6)$$

where explicit expressions⁸⁸ for C and D have been given by Rodriguez et al. in terms of the parameters given in Figure 7A. The values of C and D can be obtained empirically by fitting data of known thickness or theoretically using known values of the dielectric properties. Figure 8 shows zero-order transmission curves at perpendicular incidence for Ni mesh with 15–105 nm thick TiO₂ coatings on one side of the mesh using a

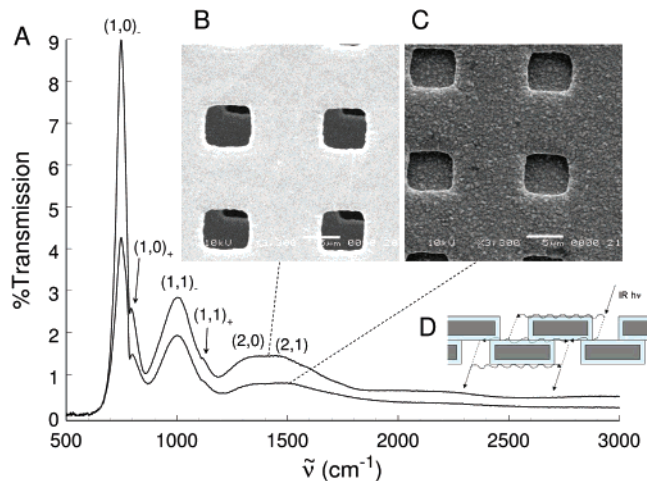


Figure 9. (A) Zero-order transmission spectra at perpendicular incidence of the two mesh stacks pictured with SEMs in panels B and C. The mesh stack in panel C has zero surface area with direct paths (it is a mirror at most wavelengths) and yet a working quantity of radiation is passed through the mid-IR. The enhancement, by the criteria of transmittance divided by fraction open surface area, is infinite. (D) Schematic of SP paths through a double stack.

Veeco/Telemark E-Beam Evaporator.⁸⁹ The thicknesses were determined by a quartz crystal capacitive microbalance with an uncertainty of ± 2 nm. The shifts of several resonances from the uncoated position vs thickness are inset at right in Figure 8. The SP resonances are clearly sensitive to nanoscale coatings of TiO_2 and the $(1,0)_+$ resonance has been fit to eq 6 giving $\Delta\tilde{\nu}_{(1,0)_+} = 0.70\tilde{\nu}^2d_2 + 32\tilde{\nu}^3d_2^2$, where $\Delta\tilde{\nu}_{(1,0)_+}$ and $\tilde{\nu}$ are in cm^{-1} and d_2 is in cm. The shift of -6.2 cm^{-1} in the data at $d_2 = 105 \text{ nm}$ can also be simulated with dielectric values for the Ni/NiO system and anatase TiO_2 producing eq 6 constants which were not far from the empirically fitted parameters. Without an NiO coating, these equations predict a shift of only -2.0 cm^{-1} at $d_2 = 105 \text{ nm}$ (rather than the observed -6.2 cm^{-1}), so the NiO coating enhances the effect over bare metal (as is known for SiO_2 coatings⁹⁰ with coupled plasmon-waveguide resonators). The $(1,0)_-$ resonance without a TiO_2 coating is shifted by an average of 36.5 cm^{-1} from the $(1,0)_+$ resonance on these meshes, primarily due to radiation damping. This value is ~ 6 times greater than the largest change observed due to TiO_2 coating, so radiation damping is very important with meshes. The “-” resonances are clearly more sensitive to nanocoatings, so there is a need for theory which addresses radiation damping on hole arrays in a manner analogous to Pockrand’s $k_x^{(1)R} + k_x^{(2)R}$ terms for SP ATR [eq 5]. This preliminary work suggests the feasibility of using the shifts of mesh transmission resonances to determine the thickness and dielectric properties of thin coatings.

2.4. Double Stacks. The role of SPs in mesh transmission is more dramatic when studies are pursued on stacks of two meshes. An enhancement factor for Ebbesen’s extraordinary transmission effect has been characterized by the ratio of transmittance to the fraction of hole surface area, and values as high as 7 have been observed⁹¹ for a single piece of mesh. A stack of two meshes was arranged in registry with zero area of direct paths for light⁶⁶ (see SEM image of Figure 9C); that is, there was metal of the second mesh everywhere behind holes of the first (see Figure 9D). The zero-order transmission spectrum is shown in the lower trace of Figure 9A revealing a working quantity [$\sim 4\%$ transmission on the $(1,0)_-$ resonance] of a Fourier transform infrared (FTIR) spectrometer’s beam; that is, it exhibits an infinite enhancement factor by the above

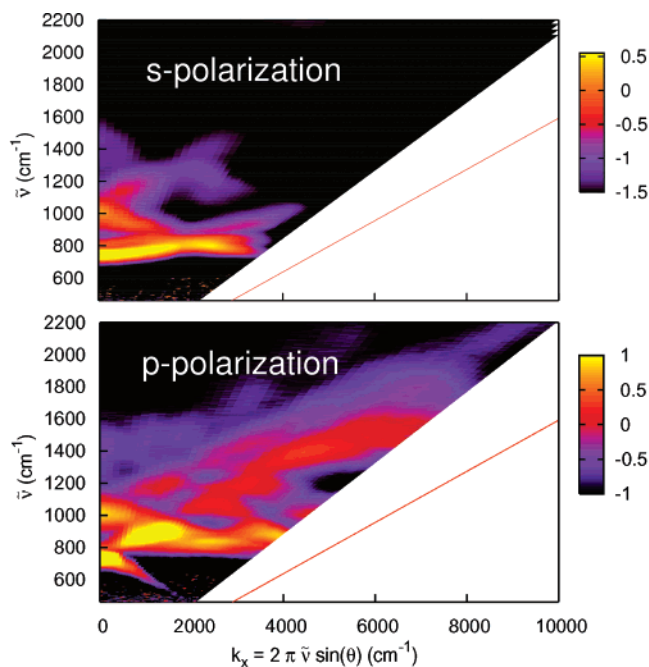


Figure 10. Dispersion plots of $\ln(\%T)$ (shown with color) vs both $\tilde{\nu}$ and k_x for s and p polarization of a 2-mesh, in-registry, double stack (as shown in Figure 9C). These plots were constructed from many zero-order transmission spectra recorded over the range $\theta = -3$ to $+45^\circ$ with geometry as defined in Figure 1B. Note that 1D arrays would typically not show any s-polarized features.

criteria. Clearly radiation must run along the surface of the metal (perpendicular to the incident beam) to get through this stack. Again, SP dispersion curves can be estimated by the perpendicular incidence method described near the end of section 2.1. The stacked arrangement reduces non-SP transmission, narrows the resonances a bit, and produces polarized dispersion plots similar to (but better defined than) that of a single piece of mesh as shown in Figure 10.⁶⁶ This can be fruitfully compared to the polarized dispersion study of Barnes et al.⁴³ in the optical region on a nanoarray. Work has been reported on mesh stacks (including a 4 mesh stack that transmits 22% of the incident light⁷⁴) in which absorption spectra are even more enhanced on double stacks than those on single meshes.⁷⁴ We have been working on double stacks of meshes coated with alkanethiol SAMs in an effort to create regions where a molecular hydrocarbon bilayer separates the two pieces of metal.

3. Topics and Applications

Several of our papers survey applications of the extraordinary transmission effect of metal meshes in the IR.^{72,74} In this section, we successively describe SP enhanced IR absorption spectroscopy of self-assembled monolayers, bilayers, and species involved in catalytic surface reactions, an interesting optical effect with mesh, interaction of SPs and molecular vibrations, and spectra recorded on individual microchannels.

3.1. Enhanced IR Absorption Spectroscopy. Perhaps the most important application³⁵ of Ebbesen’s extraordinary transmission effect in the IR is SP enhanced IR absorption (SPEIRA) spectroscopy on mesh. A brief look at other IR enhancements helps to differentiate the mesh based enhancements. Metals are well-known to facilitate surface enhanced IR absorption (SEIRA) spectroscopy,^{92–95} although the enhancements are modest (10–100) compared to those of surface enhanced Raman spectroscopy (SERS, up to perhaps 10^{14}). Since the first claims of SEIRA⁹⁶ and other early verifica-

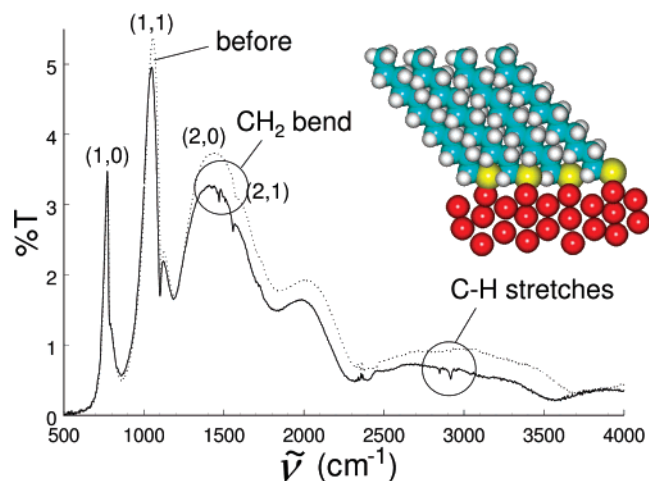


Figure 11. Zero-order transmission curves at perpendicular incidence of a Cu-coated Ni mesh before (dotted trace) and after (solid trace) dipping in dodecanethiol solution to create a self-assembled monolayer. The shift in the (1,1) resonance after coating is the wavelength scanned equivalent of SP ATR. More importantly, there are regions where molecular absorptions can be observed (circled regions) even though there is only a monolayer of sample. By picking points along the trace avoiding the molecular absorptions, a smooth spline was created and used as the background for conversion to absorption spectra (as shown in the next figure).

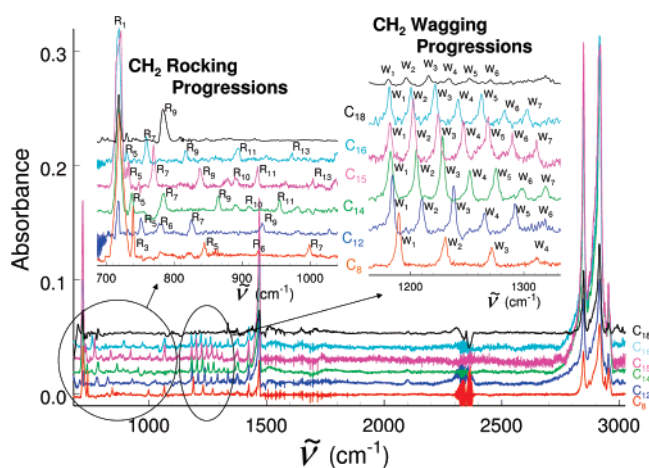


Figure 12. SPEIRA on mesh spectra of a sequence of alkanethiol SAMs with hydrocarbon chains varying from 8 to 18 carbons. The CH₂ rocking and wagging progressions (expanded) are only observed for all trans configurations of the hydrocarbon chains. The absorption in the CH stretch region is roughly 300 times that observed in RAIRS experiments. Most of these spectra were 1000 scans, at 1 cm⁻¹ resolution, with a DTGS detector.

tions,^{97,98} there has been much work^{93–95,99} explaining these enhancements. The SEIRA effect (like SERS) has both electromagnetic (buildup of E-fields at the metal interface with high dielectrics or with specific subwavelength shapes at the interface) and chemical contributions (including charge transfer to adsorbates, change in transition moments upon bonding to the metal surface,¹⁰⁰ and flow of charge from the metal to molecule in the course of a vibrational period¹⁰¹). Reflection IR absorption spectroscopy¹⁰² (RAIRS with thousands of scans) and SEIRA¹⁰³ are sufficient to study monolayers, but more enhancement opens up more spectroscopic possibilities, such as time-resolved monitoring or submonolayer monitoring.

Additional SP enhancements (both local and propagating SPs) have been reviewed³⁶ and are herein denoted as SPEIRA. Osawa et al.¹⁰⁴ showed that the localized SPs of metal islands in films contribute 200-fold enhancements over isolated molecules. SP-

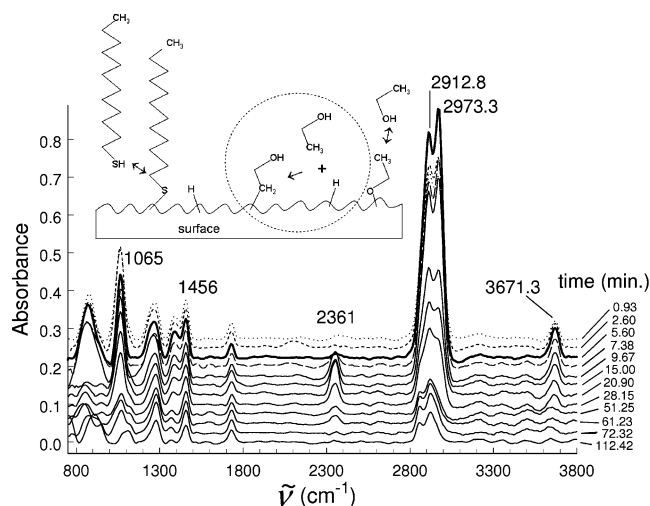


Figure 13. SPEIRA on mesh spectra of a Cu-coated mesh vs time after pulling out of an alkanethiol/ethanol solution (after two unsuccessful earlier attempts to add a SAM with alkanethiol/toluene solution). The free ethanolic OH stretch at 3671 cm⁻¹, that subsides in ~30 min, is tentatively assigned to 2-hydroxyethyl (see the circled region of inset) which could arise due to attack of ethanol solvent by H(ads). The heaviest black trace is dominated by this species.

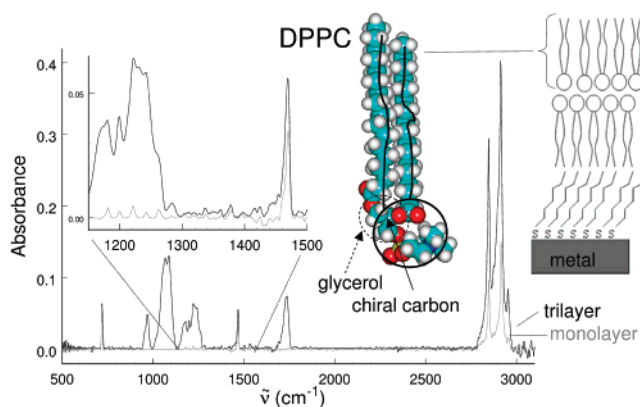


Figure 14. SPEIRA on mesh spectra of a hexadecanethiol monolayer before dipping (gray trace labeled monolayer) and after a sequence of dippings (black trace labeled trilayer) in DPPC/dichloromethane solution which assembles a bilayer of phospholipids on top of the alkanethiol monolayer. A schematic of the resulting trilayer (upper right) and a space-filling model of the DPPC molecule (center) are inset.

assisted models^{104,105} quantitatively explain the coupling between SPs of the metal films and vibrational modes of molecules adsorbed on the films.¹⁰⁶ Van Duynne and co-workers have compared enhancements of localized IR SPs on metal nanoparticles and metal island films.¹⁰⁷ Enhanced IR spectra have been recorded with wavelength-scanned SP ATR configurations.^{100,108,109} Techniques described as surface electromagnetic wave (SEW) spectroscopy^{110–113} are based on the propagation of nonradiative SP modes. Prism (or grating) coupling excites SPs out of a prism (or grating) along a smooth air/metal interface (usually with lasers), and vibrational spectra are recorded by dips in measured SP propagation lengths vs wavelength. Metal-coated edge couplers¹¹⁴ with multiple reflections can boost signal even further,⁹² including SP waveguide coupled resonators,¹¹⁵ such as the commercial BIAcore instrument.¹¹⁶

In what ways is SPEIRA with mesh different than the above-mentioned applications? Mesh arrays enable guided leaky modes (not the nonradiative mode as in SEW) to be excited at perpendicular incidence (without angling or accessories), so SP enhanced spectra can be recorded (with significant path length

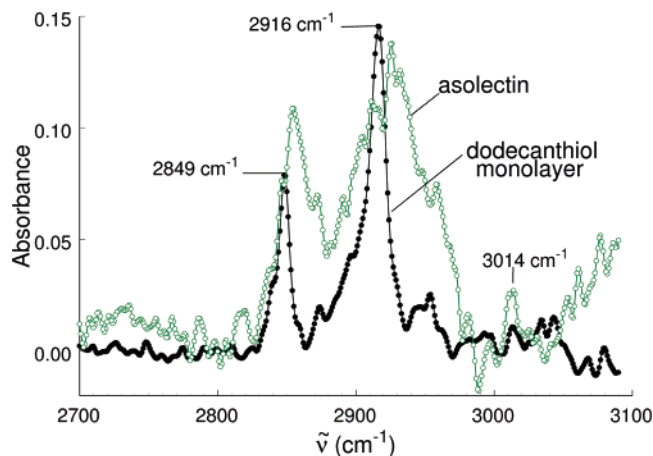


Figure 15. SPEIRA on mesh spectra of a dodecanethiol monolayer (black trace) and the same with a hydrated layer of asolectin, i.e., extract of natural phospholipids from soy bean. The blue shift of the CH stretches in the asolectin spectrum suggests that the hydrocarbon chains of the asolectin mixture are chain melted at room temperature. Note also that the CH stretch associated with C=C bonds in the chain is also detectable.

along the surface) simply by placing mesh in the sample region of standard FTIR spectrometers in transmission mode. Since mesh is considerably less expensive than coated prisms, grating couplers, or edge couplers, investigators can try configurations and/or chemistries that are too risky for expensive optics. Freestanding mesh is flexible, and curved, bent, or distorted configurations suggest new design opportunities. SPEIRA spectroscopy on mesh offers path length based enhancements of ~ 300 fold which are on top of SEIRA enhancements (10–100). Finally, note that the combination of spectroscopy with the dielectric response of SP-mediated transmission resonances (section 2.3) offers a more complete characterization of coatings.

Zero-order transmission spectra of a Cu-coated Ni mesh are shown in Figure 11 before and after coating with a self-assembled monolayer (SAM) of alkanethiol.¹⁷ In addition to small shifts of transmission resonances upon adding the one molecule thick coating, there are also molecular absorptions (circled in Figure 11). Alkanethiols with varying chain lengths (8–18 carbon atoms) were used giving rise to the sequence of absorption spectra shown in Figure 12. The CH₂ rocking and wagging progression regions (only observed for all trans configurations of the hydrocarbon chains) are expanded in Figure 12 because they have not been previously observed with other methods for alkanethiol SAMs. Both of these progressions have been analyzed in terms of coupled harmonic oscillator models showing that the vibrational force constants of these monolayers are measurably different than those of multilayers. The CH-stretch absorptions are ~ 300 -fold increased in absorption over RAIRS¹¹⁷ experiments which also have SEIRA enhancements. Spectra such as these can be recorded at different angles of the mesh relative to the spectrometer's incident beam which changes the positions and intensities of SP-transmission resonances relative to the molecular vibrations. Surprisingly, angling hardly changes the absorption spectra in the region from about 1000–4000 cm⁻¹. This suggests that most of the spectrum is dominated by some average of radiation-damped SP path-lengths. By taking the ratio of absorbances to RAIRS results,¹⁷ a path length of about 8 μm (on each side of the mesh is obtained), i.e. roughly the hole-to-hole spacing. In addition, more intense absorptions than expected can be found when the most intense transmission resonance [the (1,0)-] overlaps with a

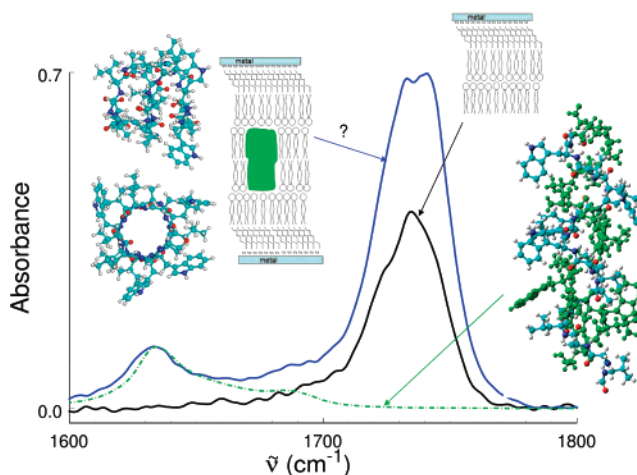


Figure 16. Future work on spectroscopic signatures of embedding in lipid bilayers. The C=O stretching region is displayed for crystalline gramicidin (green dotted trace, double helix structure), a DPPC/hexadecanethiol trilayer system (black trace, schematic at top right), and a double stack of two trilayers assembled with a drop of dilute gramicidin solution (blue trace). Since gramicidin takes on the single helix structure (at left) in membranes, we search for spectral changes that indicate incorporation into the normal, model cell membrane that can be formed in the center of the double stack (see schematic at center left).

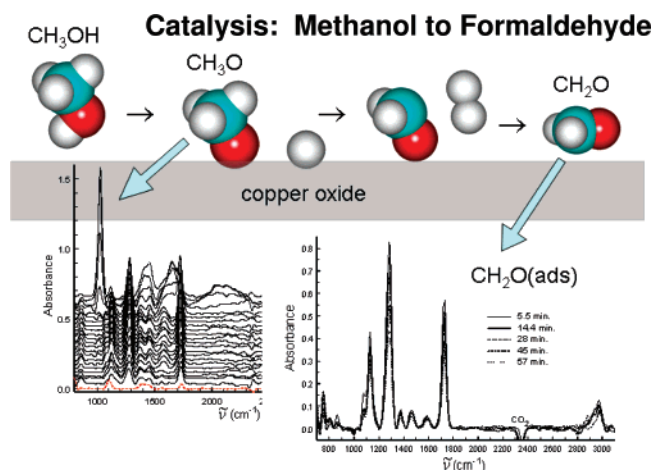


Figure 17. Reaction sequence (pictured at top) of the catalytic conversion of methanol to formaldehyde on copper oxide. SPEIRA on mesh spectra in time after adding a drop of CH₃OH (left, earliest time is at the top) to a Cu-coated and extensively oxidized mesh. The spectrum of CH₃O(ads) is observed for ~ 45 s giving way to that of CH₂O(ads) which persists for ~ 2 h. The spectrum of CH₂O(ads) is isolated at bottom right. The intensities differ much from the gas-phase suggesting interesting interactions with the metal surface.

vibration. This new and different type of enhancement will be described in more detail in section 3.4.

The process of assembling an alkanethiol monolayer involves the release of H atoms at the surface which may help to clean the surface making a higher quality SAM. We note that not every mesh produces the beautiful spectra of Figure 12 and some meshes require many iterations of treatment before producing SAMs. Figure 13 shows SP-enhanced IR absorption spectra vs time upon pulling a Cu-coated Ni mesh out of alkanethiol/ethanol solution on the third attempt after two unsuccessful initial attempts. There is a free ethanolic OH stretch (3671 cm⁻¹) that goes away in about 30 min which is tentatively assigned as due to 2-hydroxyethyl adsorbed on the surface (see inset of Figure 13 and spectrum associated with the heaviest trace). It arises due to attack of ethanol solvent by H(ads). The

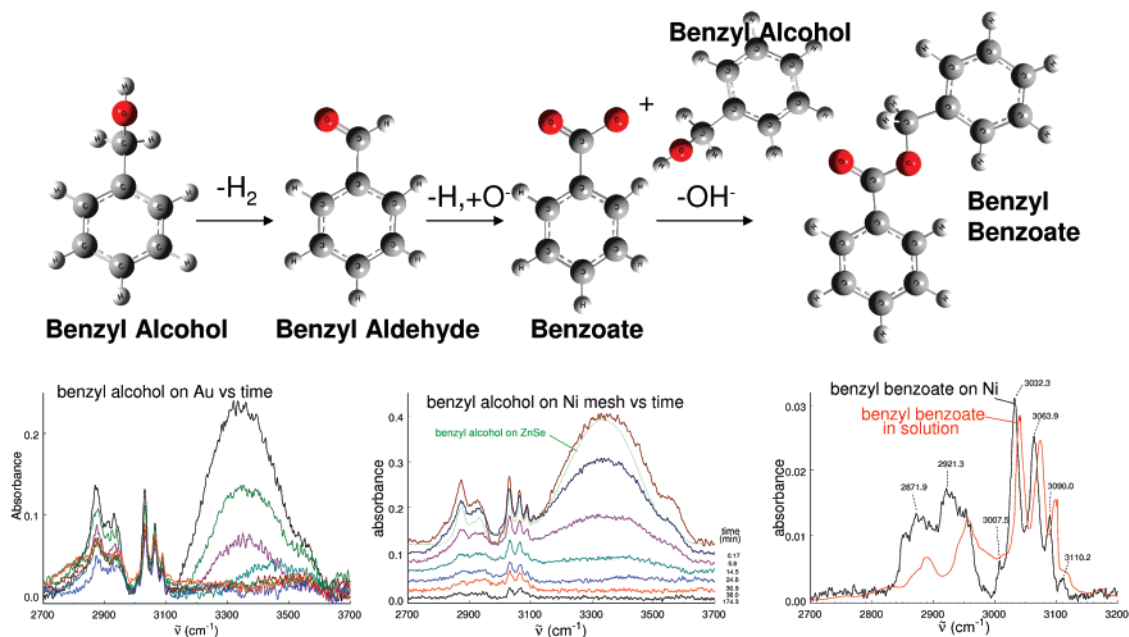


Figure 18. Catalytic reaction of benzyl alcohol to benzylbenzoate (pictured at top). SPEIRA on mesh spectra in time after adding a drop of benzyl alcohol to Au mesh (bottom left) and Ni mesh (bottom middle). The OH stretch of the alcohol diminishes as the spectrum of benzyl benzoate arises. The spectrum of benzyl benzoate on Ni is compared to the same in solution (bottom right).

2-hydroxyethyl radical has only rarely been observed spectroscopically.^{118,119} This work shows that there are unexplored opportunities regarding H(ads) surface chemistry and potential in the method for time-resolved spectroscopy.

Once an alkanethiol is applied, it becomes possible to add a phospholipid bilayer.^{72,74,120} A spectrum of a dipalmitoylphosphatidylcholine (DPPC) bilayer (reverse from that in a cell membrane) on a hexadecanethiol monolayer is shown in Figure 14. The phase, orientation, and amount of phospholipid can be followed by recording IR spectra. We are working on assessing thickness of the phospholipid layers by a combination of both ratios of the system's absorption in the CH stretch region relative to monolayers and the shifts in the (1,0)-resonance upon coating¹²⁰ (although much calibration work is still required to realize this objective). The top phospholipid layer can be removed by dipping the system in water.¹²⁰ At room temperature the hydrocarbon chains of the DPPC bilayers are not melted, whereas in biologically active membranes, the hydrocarbon chains are fluid. If an extract of natural phospholipids from soy bean is used (asolectin), the mixture is observed to be chain-melted at room temperature as revealed in the enhanced IR absorption spectra of Figure 15. Recently, we have shown that the phase of optically active DPPC phospholipid monolayers can be used as an optothermal switch to control the flow of polarized light through microchannels.¹²⁰ Note that IR SPs were used to characterize the nanoscale coatings rather than perform the optical switching which has already been accomplished¹²¹ in the visible with nanoarrays. Work continues on establishing spectroscopic signatures for incorporation of cholesterol and the peptide antibiotic gramicidin⁷⁴ (see Figure 16) into phospholipid bilayers created by double stacks of mesh coated with phospholipids. Double stacks of phospholipid bilayers on alkanethiol SAMs (see left inset of Figure 16) can produce one cell membrane-like bilayer which may even be able to be isolated or "floated" by adding water⁷² (see Figure 5 therein). Molecules trapped between two metal plates are subject to surface selection rules¹²² favoring transition moments perpendicular to the surface. Molecules oriented by, for instance, a lipid bilayer system can have relative intensities of certain vibrations varying from the

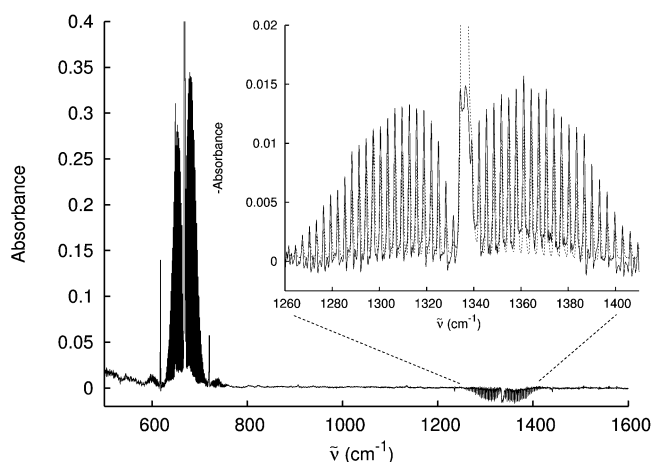


Figure 19. Double modulated signals in FTIR. An absorption spectra of the bending fundamental of CO₂(g) (~670 cm⁻¹) was recorded with a metal mesh at perpendicular incidence in the sample region of the spectrometer. The concentration of CO₂(g) was enhanced with a small chip of "dry ice", CO₂(s) in the sample region. Remarkably, the band also appears at twice the frequency and 180° out of phase (going downward). The fundamental is overlaid at twice the frequency with the inverted, double-modulated signal in the inset showing that they are the same.

random orientation prediction. We believe that there is potential here for incisive spectroscopic study of the amount, phase, and orientation of various biomolecules that might be added to model cell membranes.

3.2. Reactions: IR Spectra of Radicals, Intermediates, and Adsorbed Species. There has been much success in recording spectra of radicals, intermediates, and adsorbed species in catalytic processes at the surface of the metal mesh. A drop of methanol on an oxidized Cu-coated mesh displays the SP-enhanced spectrum of adsorbed methoxy radical intermediate for ~45 s before converting to adsorbed formaldehyde⁷⁸ which lasts for ~2 h (see Figure 17). We are currently investigating the effect of the metal surface on the intensities of the vibrations, as well as the possibility of large SP fields affecting the IR spectra. Data has also been acquired on the catalytic transforma-

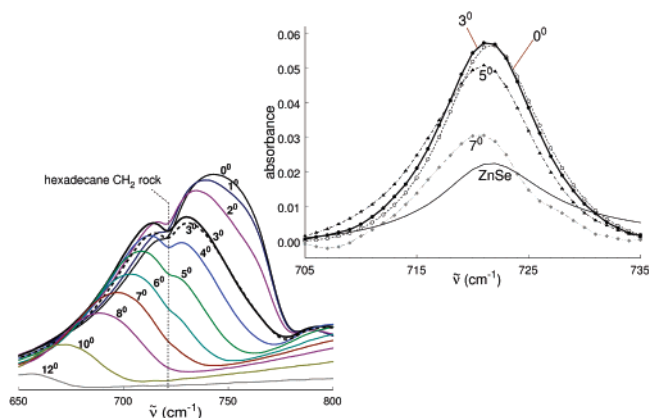


Figure 20. Transmission spectra (left) of the (1,0) resonance at different angles (θ) of a Ni mesh with a static and submicron coating of hexadecane. When the resonance is near the hexadecane CH_2 rocking vibration at 721 cm^{-1} , a dip due to SP enhanced absorption is evident. Selected spectra were worked-up in absorption (top right) showing that the SP resonance can change the intensity, position, and line shape of the vibrational feature.

tion of benzyl alcohol to benzyl benzoate on Au^{123} and Ni (see Figure 18) including the observation of benzaldehyde and benzoate intermediates. The deposition of alkanethiol SAMs has also yielded transitory spectral behaviors including the observation of 2-hydroxyethyl (ads) as shown in Figure 13, as well as SO_2 and SO_3 intermediate products in the oxidative destruction of such SAMs.

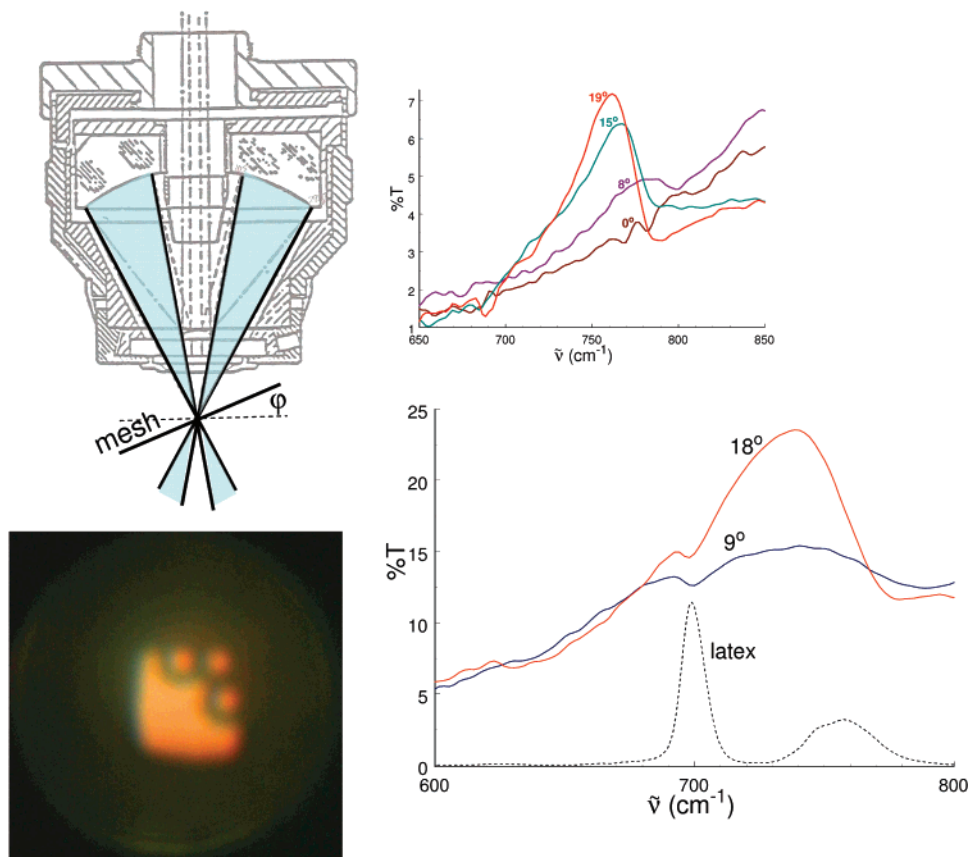


Figure 21. IR microscopes typically use reflective objectives (as pictured at top left) in which the central rays are blocked (typical pencils are shown in blue). This can severely disperse the primary transmission resonance. By tilting the mesh (by the angle ϕ), half of the rays can be brought close to perpendicular incidence which recovers the (1,0) transmission resonance as shown on the upper right. Future work will involve placing latex spheres in and about the microchannels of the mesh (as shown in the $16\text{ }\mu\text{m}$ -wide, optical microscope image with $2\text{ }\mu\text{m}$ diameter spheres at bottom left). Transmission spectra of a single microchannel with multiple latex spheres ($16.5\text{ }\mu\text{m}$ effective aperture) at two different tilt angles are shown at the bottom right, overlaid with the absorption spectrum of latex. Dips in the single-microchannel traces due to latex at 698 cm^{-1} are clearly evident, even though the rest of the spectrum is hard to detect. SP enhancements have the potential to make single microchannel IR absorption spectra routine.

3.3. Interesting Optical Effect with Mesh: Double Modulated Signals in FTIR. Mesh is a flexible building block for plasmonics. It can be stacked or readily integrated into other optical or sensing devices. In this section, a problematic example is discussed. Although most of our spectroscopic work involves radiation at perpendicular incidence that is transmitted by the mesh, the reflected beam can also come into play. Radiation that has been modulated by the FTIR spectrometer can bounce directly back from the mesh into the interferometer where it becomes double modulated. Remarkably, some of this double modulated radiation re-impinges on the mesh and is transmitted, ending up on the detector.⁶⁵ The bending fundamental band of CO_2 [which was enhanced by adding vapor from $\text{CO}_2(\text{s})$] ends up occurring at twice the frequency and 180° out of phase (going downward instead of upward as shown in Figure 19). The normal signal and double modulated signal (plotted at half the frequency and multiplied by -1) are shown in the inset of Figure 19. It is fairly rare to be able to work with light reflected perpendicularly in an FTIR spectrometer. This observation is mentioned on the chance that someone might be able to use the effect. In any case, beware of the possibility of double modulated signals.

3.4. Interaction of SPs and Vibrations. The position of SP transmission resonances can be tuned by the spacing between the holes of the array (L), the thickness⁸⁸ (section 2.3) of a coating, or by changing the angle of the mesh relative to the incident radiation beam (section 2.1). What, if anything, happens

when the most prominent SP resonance is tuned through a molecular vibration? Transmission spectra of the (1,0)₋ resonance of a Ni mesh with a static hexadecane coating of sub- μm thickness is shown in Figure 20 (lower left) at different incident angles (θ) from 0° to 12°. The resonance occurs at different positions relative to the 721 cm^{-1} CH₂ rocking vibration of hexadecane. Corresponding absorption spectra at selected angles are given in the upper right of Figure 20. Even though the amount of absorbing material is not changing, the strength, shape, and position of the absorption band changes as a function of the position of the (1,0)₋ SP resonance. A more complete study using thickness tuning has recently been accomplished⁸⁸ and systematic shifts of the CH₂ rocking vibration as a function of the position of the (1,0)₋ resonance as large as a few cm^{-1} have been observed. Since comparable shifts are observed in vibrational Stark spectroscopy with MV/cm electric fields, we wonder if the SPs can be building fields of this size at the metal surface. Interactions of this sort have also been seen with excitonic molecular states and visible SPs (both in ATR^{30,124,125} and on mesh^{121,126}), but we believe that this is the first spectroscopic observation of the interaction of a SP and an excited vibrational state. Previously, we have angled mesh to disperse the SP transmission resonances,^{78,120} and the enhanced IR absorption spectra do not change much in the region from 900 to 3500 cm^{-1} , i.e., away from the primary resonance. No doubt, one important part of previously observed enhancements is the μm -scale pathlengths for absorption enabled by SPs traveling along the surface. This new enhancement lies on top of the SP path length enhancement and provides further motivation to the idea of creating mesh with lattice parameters (L) tuned to vibrations of interest. Metal mesh patterns on silicon by Lee^{46,47,80} and co-workers demonstrate the feasibility of this idea.

3.5. Spectra of Individual Microchannels. The enhancements of SPEIRA on mesh can also be used to record spectra from spatially limited regions. Note that a 16 μm wide field of an IR microscope can isolate a single microchannel. There is a complication because the use of reflective objectives (upper left of Figure 21) in IR microscopes projects a range of nonzero incident angles at the sample (see the blue pencil of rays in upper left of Figure 21) which can obscure SP transmission resonances. A mount was built to angle the microscope's mesh sample (φ in upper left of Figure 21) such that perpendicular incidence could be obtained (for half of the incident radiation) in spite of the objective. The upper right side of Figure 21 shows different angles tuning the position of the (1,0)₋ resonance, where a mesh tilt angle of $\varphi = 18^\circ$ obtains behavior close to $\theta = 0$ as described earlier. The prominent (1,0)₋ SP resonance was tuned into overlap (lower right of Figure 21) with the most prominent vibration (698 cm^{-1}) of latex for several latex spheres trapped in the microchannel (see image at lower left of Figure 21). Clearly it will be possible to record enhanced IR absorption spectra of individual microchannels. Future work will involve coating the latex spheres with gold which does not generally reduce the IR transmission of microchannels. We will be looking for subwavelength regions that might be "hot spots" for SPEIRA and SERS methods.

4. Conclusion

Metal films with microarrays of subwavelength holes offer a very simple way to excite propagating SPs, namely by placing the mesh in the sample region of a standard FTIR spectrometer operated in transmission mode. The extraordinary transmission of these meshes enables a SP-path length-enhanced IR absorp-

tion spectroscopy, as well as characterization of the thickness and dielectric properties of nanoscale coatings. The basics of tuning SP transmission resonances have been presented and used to characterize a new type of enhancement associated with the interaction of a SP and a molecular vibration. The large absorption enhancements observed for small amounts of sample suggests potential for use with IR absorption spectroscopy in the time domain or on spatially miniscule regions, i.e., microspectroscopy.

Acknowledgment. We thank the National Science Foundation for support of this work under Grant No. CHE-0413077 and the ACS PRF under Grant Nos. 38502-AC5 and 42452-AC5.

References and Notes

- (1) Barnes, W. L.; Dereux, A.; Ebbesen, T. W. *Nature (London)* **2003**, *424*, 824.
- (2) Fang, N.; Lee, H.; Sun, C.; Zhang, X. *Science (Washington, D. C. 1883-)* **2005**, *308*, 534.
- (3) Fang, N.; Liu, Z.; Yen, T.-J.; Zhang, X. *Opt. Express* **2003**, *11*, 682.
- (4) Fang, N.; Zhang, X. *Appl. Phys. Lett.* **2003**, *82*, 161.
- (5) Yin, L.; Vlasko-Vlasov, V. K.; Rydyk, A.; Pearson, J.; Welp, U.; Chang, S.-H.; Gray, S. K.; Schatz, G. C.; Brown, D. B.; Kimball, C. W. *Appl. Phys. Lett.* **2004**, *85*, 467.
- (6) Glass, N. E.; Maradudin, A. A.; Celli, V. *Phys. Rev. B: Condens. Matter Mater. Phys.* **1983**, *27*, 5150.
- (7) Hao, E.; Schatz, G. C. *J. Chem. Phys.* **2004**, *120*, 357.
- (8) Schatz, G. C.; Young, M.; Duyne, R. P. V. Electromagnetic mechanism of SERS. In *Surface Enhanced Raman Scattering: Physics and Applications, Springer Topics in Applied Physics*; Kneipp, K., Moskovits, M., Kneipp, H., Eds.; Springer: New York, 2006; Vol. 103, pp 19.
- (9) Campion, A.; Kambampati, P. *Chem. Soc. Rev.* **1998**, *4*, 241.
- (10) Vo-Dinh, T. *TrAC Trends Anal. Chem.* **1998**, *17*, 557.
- (11) Ozbay, E. *Science (Washington, DC)* **2006**, *311*, 189.
- (12) Rendell, R. W.; Scalapino, D. J. *Phys. Rev. B* **1981**, *24*, 3276.
- (13) Haes, A. J.; Van Duyne, R. P. *Anal. Bioanal. Chem.* **2004**, *379*, 920.
- (14) Lakowicz, J. R. *Anal. Biochem.* **2004**, *324*, 153.
- (15) Brolo, A. G.; Kwok, S. C.; Moffitt, M. G.; Gordon, R.; Riordon, J.; Kavanagh, K. L. *J. Am. Chem. Soc.* **2005**, *127*, 14936.
- (16) Ebbesen, T. W.; Lezec, H. J.; Ghaemi, H. F.; Thio, T.; Wolff, P. A. *Nature (London)* **1998**, *391*, 667.
- (17) Rodriguez, K. R.; Shah, S.; Williams, S. M.; Teeters-Kennedy, S.; Coe, J. V. *J. Chem. Phys.* **2004**, *121*, 8671.
- (18) Maestre, D. *Selected papers on diffraction gratings*; SPIE Optical Engineering Press: Bellingham, WA, 1993.
- (19) Wood, R. W. *Philos. Mag.* **1902**, *4*, 396.
- (20) Strong, J. *Phys. Rev.* **1936**, *49*, 291.
- (21) Rayleigh, L. *Philos. Mag. Series 6* **1907**, *14*, 60.
- (22) Fano, U. *J. Opt. Soc. Am.* **1941**, *31*, 213.
- (23) Sommerfeld, A. *Ann. Phys.* **1909**, *28*, 665.
- (24) Ritchie, R. H. *Phys. Rev.* **1957**, *106*, 874.
- (25) Ferrell, R. A. *Phys. Rev.* **1958**, *111*, 1214.
- (26) Powell, C. J.; Swan, J. B. *Phys. Rev.* **1960**, *118*, 640.
- (27) Steinmann, W. *Phys. Rev. Lett.* **1960**, *5*, 470.
- (28) Steinmann, W. *Z. Phys.* **1961**, *163*, 92.
- (29) Teng, Y.-Y.; Stern, E. *Phys. Rev. Lett.* **1967**, *19*, 511.
- (30) Raether, H. *Surface plasmons on smooth and rough surfaces and on gratings*; Springer-Verlag: Berlin, 1988.
- (31) Ritchie, R. H.; Arakawa, E. T.; Cowan, J. J.; Hamm, R. N. *Phys. Rev. Lett.* **1968**, *21*, 1530.
- (32) Hutley, M. C.; Bird, M. V. M. *Opt. Acta* **1973**, *20*, 771.
- (33) Otto, A. *Z. Phys.* **1968**, *216*, 398.
- (34) Kretschmann, E.; Raether, H. *Z. Naturforsch.* **1968**, *23*, 2135.
- (35) Genet, C.; Ebbesen, T. W. *Nature (London)* **2007**, *445*, 39.
- (36) Andersen, P. C.; Rowlen, K. L. *Appl. Spectrosc.* **2002**, *56*, 124A.
- (37) Pockrand, I. *Surf. Sci.* **1978**, *72*, 577.
- (38) Welford, K. R.; Sambles, J. R. *J. Mod. Opt.* **1988**, *35*, 1467.
- (39) Garcia-Vidal, F. J.; Martin-Moreno, L.; Pendry, J. B. *J. Opt. A* **2005**, *7*, S97.
- (40) Ulrich, R. Modes of Propagation on an Open Periodic Waveguide for the Far Infrared. *Optical and Acoustical Micro-electronics*; Polytechnic Press: New York, 1974.
- (41) Bethe, H. A. *Phys. Rev.* **1944**, *66*, 163.
- (42) Ghaemi, H. F.; Thio, T.; Grupp, D. E.; Ebbesen, T. W.; Lezec, H. *J. Phys. Rev. B* **1998**, *58*, 6779.

- (43) Barnes, W. L.; Murray, W. A.; Dintinger, J.; Devaux, E.; Ebbesen, T. W. *Phys. Rev. Lett.* **2004**, *92*, 107401/1.
- (44) Kwak, E.-S.; Henzie, J.; Chang, S.-H.; Gray, S. K.; Schatz, G. C.; Odom, T. W. *Nano Lett.* **2005**, *5*, 1963.
- (45) Williams, S. M.; Coe, J. V. *Plasmonics* **2006**, *1*, 87.
- (46) Tsai, M.-W.; Chuang, T.-H.; Chang, H.-Y.; Lee, S.-C. *Appl. Phys. Lett.* **2006**, *88*, 213112/1.
- (47) Tsai, M.-W.; Chuang, T.-H.; Chang, H.-Y.; Lee, S.-C. *Appl. Phys. Lett.* **2006**, *89*, 093102/1.
- (48) Thio, T.; Ghaemi, H. F.; Lezec, H. J.; Wolff, P. A.; Ebbesen, T. W. *J. Opt. Soc. Am. B* **1999**, *16*, 1743.
- (49) Naweed, A.; Baumann, F.; Bailey, W. A., Jr.; Karakashian, A. S.; Goodhue, W. D. *J. Opt. Soc. Am. B* **2003**, *20*, 2534.
- (50) Kim, D. S.; Hong, S. C.; Malyarchuk, V.; Yoon, Y. C.; Ahn, Y. H.; Lee, K. J.; Park, J. W.; Kim, J.; Park, Q. H.; Lienau, C. *Phys. Rev. Lett.* **2003**, *91*, 143901/1.
- (51) van der Molen, K. L.; Klein Koerkamp, K. J.; Enoch, S.; Segerink, F. B.; van Hulst, N. F.; Kuipers, L. *Phys. Rev. B* **2005**, *72*, 045421/1.
- (52) Degiron, A.; Lezec, H. J.; Yamamoto, N.; Ebbesen, T. W. *Opt. Commun.* **2004**, *239*, 61.
- (53) Koerkamp, K. J. K.; Enoch, S.; Segerink, F. B.; Van Hulst, N. F.; Kuipers, L. *Phys. Rev. Lett.* **2004**, *92*, 183901/1.
- (54) Van der Molen, K. L.; Segerink, F. B.; Van Hulst, N. F.; Kuipers, L. *Appl. Phys. Lett.* **2004**, *85*, 4316.
- (55) Gordon, R.; Brolo, A. G.; McKinnon, A.; Rajora, A.; Leathem, B.; Kavanagh, K. L. *Phys. Rev. Lett.* **2004**, *92*, 037401/1.
- (56) Gordon, R.; Hughes, M.; Leathem, B.; Kavanagh, K. L.; Brolo, A. G. *Nano Lett.* **2005**, *5*, 1243.
- (57) Dogariu, A.; Thio, T.; Wang, L. J.; Ebbesen, T. W.; Lezec, H. J. *Opt. Lett.* **2001**, *26*, 450.
- (58) Altewischer, E.; van Exter, M. P.; Woerdman, J. P. *Nature (London)* **2002**, *418*, 304.
- (59) Altewischer, E.; Genet, C.; Exter, M. P. v.; Woerdman, J. P.; Zuuk, A. v.; Drift, E. W. J. M. v. d. *Opt. Lett.* **2005**, *30*, 90.
- (60) Genet, C.; Altewischer, E.; van Exter, M. P.; Woerdman, J. P. *Phys. Rev. B* **2005**, *71*, 033409/1.
- (61) Popov, E.; Neviere, M.; Enoch, S.; Reinisch, R. *Phys. Rev. B* **2000**, *62*, 16100.
- (62) Martin-Moreno, L.; Garcia-Vidal, F. J.; Lezec, H. J.; Pellerin, K. M.; Thio, T.; Pendry, J. B.; Ebbesen, T. W. *Phys. Rev. Lett.* **2001**, *86*, 1114.
- (63) Lalanne, P.; Rodier, J. C.; Hugonin, J. P. *J. Opt. A* **2005**, *7*, 422.
- (64) Jia, W.; Liu, X. *Eur. Phys. J. B* **2005**, *46*, 343.
- (65) Williams, S. M. Characteristics and Applications of the Infrared Enhanced Transmission of Metallic Subwavelength Arrays. Ph.D., The Ohio State University: Columbus, OH, 2006.
- (66) Teeters-Kennedy, S. M.; Williams, S. M.; Rodriguez, K. R.; Cilwa, K.; Meleason, D.; Sudnitsyn, A.; Hrovat, F.; Coe, J. V. *J. Phys. Chem. C* **2007**, *111*, 124.
- (67) Devaux, E.; Ebbesen, T. W.; Weeber, J.-C.; Dereux, A. *Appl. Phys. Lett.* **2003**, *83*, 4936.
- (68) Murray, W. A.; Astilean, S.; Barnes, W. L. *Phys. Rev. B* **2004**, *69*, 165407/1.
- (69) Moller, K. D.; Sternberg, O.; Grebel, H.; Lalanne, P. *J. Appl. Phys.* **2002**, *91*, 9461.
- (70) Moller, K. D.; Farmer, K. R.; Ivanov, D. V. P.; Sternberg, O.; Stewart, K. P.; Lalanne, P. *Infrared Phys. Technol.* **1999**, *40*, 475.
- (71) Williams, S. M.; Stafford, A. D.; Rodriguez, K. R.; Rogers, T. M.; Coe, J. V. *J. Phys. Chem. B* **2003**, *107*, 11871.
- (72) Coe, J. V.; Williams, S. M.; Rodriguez, K. R.; Teeters-Kennedy, S.; Sudnitsyn, A.; Hrovat, F. *Anal. Chem.* **2006**, *March 1*, 1385.
- (73) Williams, S. M.; Stafford, A. D.; Rogers, T. M.; Bishop, S. R.; Coe, J. V. *Appl. Phys. Lett.* **2004**, *85*, 1472.
- (74) Williams, S. M.; Rodriguez, K. R.; Teeters-Kennedy, S.; Shah, S.; Rogers, T. M.; Stafford, A. D.; Coe, J. V. *Nanotechnology* **2004**, *15*, S495.
- (75) Teeters-Kennedy, S. M. The Extraordinary Transmission of Subwavelength Metallic Arrays: An Infrared Study of the Self-Assembly of Phospholipid Bilayers on Alkanethiol Monolayers. M.S. thesis, The Ohio State University: Columbus, OH, 2004.
- (76) Rodriguez, K. R.; Teeters-Kennedy, S. M.; Williams, S. M.; Coe, J. V. **2007**, to be submitted.
- (77) Rodriguez, K. R.; Meleason, D. S.; Coe, J. V. *J. Phys. Chem. B* **2007**, *2007*, to be submitted.
- (78) Williams, S. M.; Rodriguez, K. R.; Teeters-Kennedy, S.; Stafford, A. D.; Bishop, S. R.; Lincoln, U. K.; Coe, J. V. *J. Phys. Chem. B* **2004**, *108*, 11833.
- (79) Tsai, M.-W.; Chuang, T.-H.; Meng, C.-Y.; Chang, Y.-T.; Lee, S.-C. *Appl. Phys. Lett.* **2006**, *89*, 173116/1.
- (80) Chuang, T.-H.; Tsai, M.-W.; Chang, Y.-T.; Lee, S.-C. *Appl. Phys. Lett.* **2006**, *89*, 033120/1.
- (81) Chuang, T.-H.; Tsai, M.-W.; Chang, Y.-T.; Lee, S.-C. *Appl. Phys. Lett.* **2006**, *89*, 173128/1.
- (82) Liu, Z.; Durant, S.; Lee, H.; Xiong, Y.; Pikus, Y.; Sun, C.; Zhang, X. *Opt. Lett.* **2007**, *32*, 629.
- (83) Economou, E. N. *Phys. Rev.* **1969**, *182*, 539.
- (84) Yang, F.; Bradberry, G. W.; Sambles, J. R. *J. Mod. Opt.* **1990**, *37*, 993.
- (85) Fuzi, Y.; Bradberry, G. W.; Sambles, J. R. *J. Mod. Opt.* **1989**, *36*, 1405.
- (86) Rakic, A. D.; Djuricic, A. B.; Elazar, J. M.; Majewski, M. L. *Appl. Opt.* **1998**, *37*, 5271.
- (87) Degiron, A.; Lezec, H. J.; Barnes, W. L.; Ebbesen, T. W. *Appl. Phys. Lett.* **2002**, *81*, 4327.
- (88) Rodriguez, K. R.; Tian, H.; Heer, J. M.; Teeters-Kennedy, S. M.; Cilwa, K.; Coe, J. V. *J. Chem. Phys.* **2007**, *126*, 151101/1.
- (89) Rodriguez, K. R.; Tian, H.; Heer, J. M.; Coe, J. V. *J. Phys. Chem. C* **2007**, *111*, 12106.
- (90) Salamon, Z.; Macleod, H. A.; Tollin, G. *Biophys. J.* **1997**, *73*, 2791.
- (91) Lezec, H. J.; Thio, T. *Opt. Express* **2004**, *12*, 3269.
- (92) Suetaka, W. *Surface Infrared and Raman Spectroscopy: Methods and Applications*; Plenum Press: New York, 1995; Vol. 3.
- (93) Aroca, R. F.; Ross, D. J.; Domingo, C. *Appl. Spectrosc.* **2004**, *58*, 324A.
- (94) Osawa, M. *Bull. Chem. Soc. Jpn.* **1997**, *70*, 2861.
- (95) Osawa, M.; Ataka, K.-I.; Yoshi, K.; Nishikawa, Y. *Appl. Spectrosc.* **1993**, *47*, 1497.
- (96) Hartstein, A.; Kirtley, J. R.; Tsang, J. C. *Phys. Rev. Lett.* **1980**, *45*, 201.
- (97) Hatta, A.; Ohshima, T.; Suetaka, W. *Appl. Phys. A* **1982**, *A21*, 71.
- (98) Hatta, A.; Suzuki, Y.; Suetaka, W. *Appl. Phys. A* **1984**, *A35*, 135.
- (99) Aroca, R.; Price, B. *J. Phys. Chem. B* **1997**, *101*, 6537.
- (100) Badilescu, S.; Ashrit, P. V.; Vo Van, T.; Badilescu, I. I. *Appl. Spectrosc.* **1989**, *43*, 549.
- (101) Feibelman, P. J. *Annu. Rev. Phys. Chem.* **1989**, *40*, 261.
- (102) Allara, D. L.; Nuzzo, R. G. *Langmuir* **1985**, *1*, 52.
- (103) Johnson, E.; Aroca, R. *J. Phys. Chem.* **1995**, *99*, 9325.
- (104) Osawa, M.; Ataka, K.; Yoshii, K.; Nishikawa, Y. *Appl. Spectrosc.* **1993**, *47*, 1497.
- (105) Osawa, M. *Bunko Kenkyu* **1993**, *42*, 127.
- (106) Osawa, M. *Top. Appl. Phys.* **2001**, *81*, 163.
- (107) Jensen, T. R.; Van Duyne, R. P.; Johnson, S. A.; Maroni, V. A. *Appl. Spectrosc.* **2000**, *54*, 371.
- (108) Delgado, J. M.; Orts, J. M.; Rodes, A. *Langmuir* **2005**, *21*, 8809.
- (109) Anariba, F.; Viswanathan, U.; Bocian, D. F.; McCreery, R. L. *Anal. Chem.* **2006**, *78*, 3104.
- (110) Zhizhin, G. N.; Vinogradov, E. A.; Moskalova, M. A.; Yakovlev, V. A. *Appl. Spectrosc. Rev.* **1982-83**, *18*, 171.
- (111) Zhizhin, G. N.; Moskalova, M. A.; Vinogradov, E. A.; Sigarev, A. A.; Yakovlev, V. A. *J. Electron Spectrosc. Relat. Phenom.* **1983**, *30*, 35.
- (112) Silin, V. I.; Voronov, S. A.; Yakovlev, V. A.; Zhizhin, G. N. *Int. J. Infrared Millimeter Waves* **1989**, *10*, 101.
- (113) Alieva, E. V.; Beitel, G.; Kuzik, L. A.; Sigarev, A. A.; Yakovlev, V. A.; Zhizhin, G. N.; Meer, A. F. G. v. d.; Wiel, M. J. v. d. *Appl. Spectrosc.* **1997**, *51*, 584.
- (114) Chabal, Y. J.; Sievers, A. *J. Appl. Phys. Lett.* **1978**, *32*, 90.
- (115) Plant, A. L.; Brigham-Burke, M.; Petrella, E. C.; Oshannessy, D. *J. Anal. Biochem.* **1995**, *226*, 342.
- (116) Brigham-Burke, M.; Edwards, J. R.; O'Shannessy, D. *J. Anal. Biochem.* **1992**, *205*, 125.
- (117) Laibinis, P.; Whitesides, G. M.; Allara, D. L.; Tao, Y.-T.; Parikh, A. N.; Nuzzo, R. G. *J. Am. Chem. Soc.* **1991**, *113*, 7152.
- (118) Kuo, Y. P.; Wann, G. H.; Lee, Y. P. *J. Chem. Phys.* **1993**, *99*, 3272.
- (119) Feltham, E. J.; Almond, M. J.; Marston, G.; Wiltshire, K. S.; Goldberg, N. *Spectrochim. Acta, Part A* **2000**, *56A*, 2589.
- (120) Teeters-Kennedy, S. M.; Rodriguez, K. R.; Rogers, T. M.; Zomchek, K. A.; Williams, S. M.; Sudnitsyn, A.; Carter, L.; Cherezov, V.; Caffrey, M.; Coe, J. V. *J. Phys. Chem. B* **2006**, *110*, 21719.
- (121) Dintinger, J.; Klein, S.; Ebbesen, T. W. *Adv. Mater. (Weinheim)* **2006**, *18*, 1267.
- (122) Fan, J.; Trenary, M. *Langmuir* **1994**, *10*, 3649.
- (123) Meleason, D. Benchtop Nanotechnology: Utilizing the Extraordinary Transmission Effect to Study Alkanethiol Self Assembled Monolayers, a Gold Catalyzed Reaction, and the Construction of Nanostructures in Microchannels; The Ohio State University: Columbus, OH, 2006.
- (124) Pockrand, I.; Swalen, J. D.; II, J. G. G.; Philpott, M. R. *J. Chem. Phys.* **1979**, *70*, 3401.
- (125) Pockrand, I.; Brillante, A.; Mobius, D. *J. Chem. Phys.* **1982**, *77*, 6289.
- (126) Dintinger, J.; Klein, S.; Bustos, F.; Barnes, W. L.; Ebbesen, T. W. *Phys. Rev. B* **2005**, *71*, 035424/1.